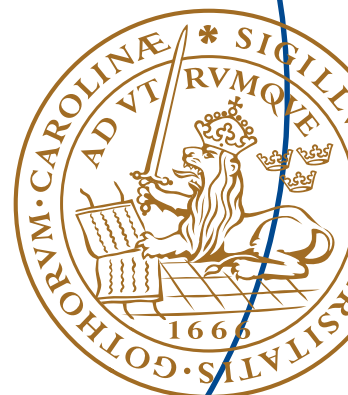


Master's Thesis

# High Precision RF Measurement for ESS Cavity Parameters

Philip Jönsson



# High Precision RF Measurement for ESS Cavity Parameters

Philip Jönsson  
atn09pjo@student.lu.se

ESS AB  
Tunavägen 24  
223 63 Lund  
Sweden

Advisor: Rihua Zeng

February 2, 2015



---

# Abstract

---

In this thesis an investigation of how inaccuracies in measurements affects the field in the cavities used in the accelerator of the European Spallation Source (ESS). New ways to calculate the dynamic detuning and the quality factor of the cavities will also be investigated. This is done by setting up a simulation model in Simulink where the cavities are described by a differential equation. This model includes both the new and old analysis methods. It is found that different inaccuracies have very different effects on the cavity. Inaccuracies in quality factor and R/Q value affect the cavity control the most.

The new calculation method for the dynamic detuning is found to be better since it can show the dynamic detuning both during and after the RF pulse and it is less dependent on inaccuracies. For  $Q_L$  the old measurement method is better since inaccuracies have less impact on it than on the new measurement method.



---

# Table of Contents

---

<b>1</b>	<b>Introduction</b>	<b>1</b>
<b>2</b>	<b>Background</b>	<b>3</b>
2.1	ESS	3
2.2	Accelerator	3
2.3	Cavity and Basic Parameters	4
2.3.1	Cavity Voltage	5
2.3.2	Loaded Q-value, $Q_L$	5
2.3.3	Beam Phase	6
2.3.4	R/Q	6
2.3.5	Dynamic Detuning	6
2.4	High Precision Measurement	7
<b>3</b>	<b>High Precision Measurement Modelling and Investigation</b>	<b>9</b>
3.1	Basic Models	9
3.1.1	Cavity Model	9
3.1.2	Lorentz Force Detuning Model	10
3.1.3	Directional Coupler Model	10
3.1.4	Feedforward Control Model	12
3.2	Get Constant Field using only Feedforward	13
3.2.1	$Q_L$ Optimization	13
3.2.2	Pre-Detuning Optimization	14
3.2.3	Injection Time Optimization	14
3.2.4	Frequency Tracking During Filling Time	15
3.2.5	Lorentz Force Detuning Compensation	15
3.3	Gradient Ramp-up Procedures	16
3.3.1	General Procedures	16
3.3.2	Ramp-up with Different Feedforward Strategies	17
3.4	Effects of Inaccurate Parameters on Ramp-up Procedures/Feedforward	18
3.4.1	Inaccurate Cavity Voltage	18
3.4.2	Inaccurate Synchronous Phase	19
3.4.3	Inaccurate R/Q	21
3.4.4	Inaccurate Quality Factor	22

3.4.5	Inaccurate Dynamic Detuning	23
<b>3.5</b>	<b>Improvement Investigation of Accuracy/Precision in System Modelling</b>	<b>23</b>
3.5.1	Hardware Limitation	23
3.5.1.1	Directivity of Directional Coupler	23
3.5.1.2	Coupling factor of the Directional Coupler	25
3.5.1.3	Resolution Limitation of Adjustable Injection Time and Pre-detuning	26
3.5.2	Measurement Algorithm Limitation	27
3.5.2.1	Detuning	27
3.5.2.2	$Q_L$	29
<b>3.6</b>	<b>Other Ways of Improving the Measurements . . . . .</b>	<b>31</b>
3.6.1	RF Power Based Calibration for $Q_L$ and Detuning	31
3.6.2	RF Based Calibration for R/Q	33
3.6.3	Beam Based Calibration for $V_{cav}$ & Phase	34
<b>4</b>	<b>Measurements</b>	<b>35</b>
4.1	Cavity Response . . . . .	35
4.2	Detuning Measurement . . . . .	36
4.2.1	Decay	36
4.3	$Q_L$ Measurement . . . . .	38
4.3.1	Decay	38
4.4	Directivity of Directional Coupler Measurement . . . . .	41
<b>5</b>	<b>Conclusion</b>	<b>43</b>
	<b>References</b>	<b>45</b>
<b>A</b>	<b>Simulink Models</b>	<b>47</b>

---

# List of Figures

---

2.1	<i>A block diagram of the accelerator [5]</i> . . . . .	4
2.2	<i>Graph of the standing wave [2].</i> . . . . .	5
2.3	<i>LCR model of the cavity, in the dashed rectangle, with an external load, <math>R_L</math>, connected. [1]</i> . . . . .	6
3.1	<i>Directional coupler.</i> . . . . .	11
3.2	<i>Model of the directional coupler in Simulink</i> . . . . .	11
3.3	<i>Feedforward model</i> . . . . .	12
3.4	<i>Amplitude</i> . . . . .	15
3.5	<i>Amplitude</i> . . . . .	15
3.6	<i>The amplitude and phase) of the iterated cavity field</i> . . . . .	16
3.7	<i>The amplitude and phase of the cavity field when just increasing the scaling factor from 0.1 to 1 and the detuning constant <math>K=30</math> Hz/MV</i> . . . . .	16
3.8	<i>The iterative loop to acquire a good cavity gradient ramp-up.</i> . . . . .	17
3.9	<i>The amplitude and phase of the cavity field with the feedforward table from the previous scaling factor when increasing the scaling factor from 0.1 to 1 and the detuning constant <math>K=30</math> Hz/MV</i> . . . . .	17
3.10	<i>The amplitude and phase of the cavity field after three iterations of the feedforward table has been done, increasing the scaling factor from 0.1 to 1 and the detuning constant <math>K=30</math> Hz/MV</i> . . . . .	18
3.11	<i>Effect of voltage errors on the amplitude and phase of the cavity field.</i> . . . . .	19
3.12	<i>Effect of voltage errors on the amplitude and phase of the cavity field after acquiring and using a new feedforward table.</i> . . . . .	19
3.13	<i>Effect of synchronous phase errors on the amplitude and phase of the cavity field.</i> . . . . .	20
3.14	<i>Effect of synchronous phase errors on the amplitude and phase of the cavity field after acquiring and using a new feedforward table.</i> . . . . .	20
3.15	<i>Effect of an <math>R/Q</math> value larger than the optimal on the amplitude and phase of the cavity field.</i> . . . . .	21
3.16	<i>Effect of an <math>R/Q</math> value smaller than the optimal on the amplitude and phase of the cavity field.</i> . . . . .	21
3.17	<i>Effect of a <math>Q_L</math> value larger than the optimal on the amplitude and phase of the cavity field.</i> . . . . .	22



3.18	<i>Effect of a <math>Q_L</math> value smaller than the optimal on the amplitude and phase of the cavity field.</i>	22
3.19	<i>Effect of dynamic detuning errors on the amplitude and phase of the cavity field.</i>	23
3.20	<i>Ideal detuning for <math>K=30</math></i>	24
3.21	<i>Effect of different directivities on the detuning</i>	24
3.22	<i>Amplitude and phase of the cavity fields for the different directivities.</i>	24
3.23	<i>Effect of a coupling factor of 60.1 dB on the cavity field.</i>	25
3.24	<i>Effect of a coupling factor of 61 dB on the cavity field.</i>	26
3.25	<i>Effect of inaccurate pre-detuning.</i>	26
3.26	<i>Effect of inaccurate injection time.</i>	27
3.27	<i>Detuning calculated with equation ?? (whole) and ?? (dashed)</i>	28
3.28	<i>Detuning calculated with equation ?? (whole) and ?? (dashed) with coupling factor 60.1 dB</i>	28
3.29	<i>Detuning calculated with equation ?? (whole) and ?? (dashed) with 30 dB directivity.</i>	29
3.30	<i>Loaded quality factor, <math>Q_L</math>, calculated with equation ?? (whole) and the input <math>Q_L</math> (dashed) with different K-values.</i>	30
3.31	<i>Loaded quality factor, <math>Q_L</math>, calculated with equation ?? (whole) and the input <math>Q_L</math> (dashed) with coupling factor 60.1 dB</i>	31
3.32	<i>Loaded quality factor, <math>Q_L</math>, calculated with equation ?? (whole) and ?? (dashed) with 30dB directivity.</i>	31
4.1	<i>Measurement setup.</i>	35
4.2	<i>Cavity response on the rising edge of a pulse.</i>	36
4.3	<i>Cavity response on the falling edge of a pulse.</i>	36
4.4	<i>Measured voltage for different phase differences at 352.21 MHz and 327.36 MHz.</i>	37
4.5	<i>The phase of the cavity field at different RF-frequencies.</i>	37
4.6	<i>How the detuning changes when the frequency is changes.</i>	38
4.7	<i>Decay measurement</i>	39
4.8	<i>Decay measurement</i>	40
4.9	<i>Effect of ratio of sampling clock to input frequency on quantization noise spectrum for ideal 12-bit ADC [16]</i>	41
4.10	<i>Sketch of the directional coupler used in the measurements</i>	42
A.1	<i>Cavity model in Simulink</i>	47
A.2	<i>The model of calculating the detuning in Simulink</i>	48

# Introduction

---

European Spallation Source (ESS) is a particle accelerator that accelerates protons to make them collide with a target to create neutrons that in turn are used to investigate other samples. The accelerator consists of many resonant cavities in series. Inside the cavities a large electric field is generated using an RF-pulse. In other particle accelerators mainly feedback control is used. This consumes more energy than using feedforward, i.e. predicting how the cavity will behave and compensate for it before the cavity is turned on. ESS has a requirement of low energy consumption so it is very important that the prediction in the feedforward is accurate. This will be done by having measuring methods that can acquire data with high precision and also improving the start-up procedures and the feedforward control methods.

The purpose of this thesis is to investigate how some factors affect the measurement results and in turn the control of the cavity. This is done by first setting up mathematical models in Simulink for the cavity and the measuring devices used for measuring important parameters. It is then investigated how different inaccuracies in measurements affects the cavity. Both the method already in use as well as an alternative method are investigated and compared to each other to determine which method is the better one, and for which parameters. Lastly some measurements will be done on a small scale prototype of the cavity.



---

# Background

---

## 2.1 ESS

European Spallation Source, ESS, is a multinational research center where 17 countries are contributing toward building the facility. The project started in 1998 when the Organization for Economic Development, OECD, decided that one high-intensity neutron source should be built in each of the continents North America, Europe and Asia. During the next ten years the project was worked out and a location for the European facility was chosen, Lund in Sweden. During the last five years the specifications and the design of the accelerator has been developed to find the optimal layout in terms of energy consumption and precision of the beam in the accelerator, and how the target station should be designed.

The idea of the project is to accelerate protons, by using electric fields, up to almost the speed of light and then let them collide with a target of tungsten. After the collision neutrons with high energy are released from the target in many directions. Then the neutrons are slowed down to approximately the speed of sound and guided into different research facilities located around the target station. In these facilities investigations of material properties are made on everything from plastics and metals to biomolecules and archaeological samples. [4] [5] The more neutrons that are released from the tungsten target the "brighter" it is, which improves the resolution of the measurement.

## 2.2 Accelerator

The accelerator in ESS is a so called Linac, Linear accelerator, which means that the accelerator is a straight line. The proton beam originates from the source with an energy of 75 keV and is then accelerated. The accelerator is divided in 8 sections starting with a low energy beam transport (LEBT) followed by a radio frequency quadrupole (RFQ) where the beam is bunched and accelerated to 3 MeV which corresponds to a velocity of approximately 8 % of the speed of light. The proton beam is then transported through a medium energy beam transport (MEBT) section where it connected to a drift tube linac (DTL) where the protons is further accelerated to 78 MeV. Now the protons travel at 38 % of the speed of light. Now the protons reach the part where they are accelerated the most, the resonant cavities. It starts with 28 Spoke cavities followed by 60 medium- $\beta$  elliptical cavities and 120 high- $\beta$  elliptical cavities.  $\beta$  is the fraction of the speed of light that the

cavity can approximately accelerate the protons to most effectively. The spoke cavities have a geometric  $\beta$  of 0.5 and working frequency of 352.21 MHz and after the 28 cavities the protons have an energy of 200 MeV, which corresponds to 57 % of the light speed. The medium- $\beta$  elliptical cavities has a geometrical  $\beta$  of 0.67 and working frequency of 704.42 MHz and after them the protons have an energy of 638 MeV, which corresponds to 80 % of the speed of light. The high- $\beta$  elliptical cavities has the same working frequency as the medium- $\beta$  elliptical cavities, i.e. 704.42 MHz, and a geometric  $\beta$  of 0.92. Now the protons have the energy 2500 MeV and are travelling with 96 % of the speed of light. After the high- $\beta$  cavities the protons are transported to the target through a High Energy Beam Transport (HEBT) segment. [5]

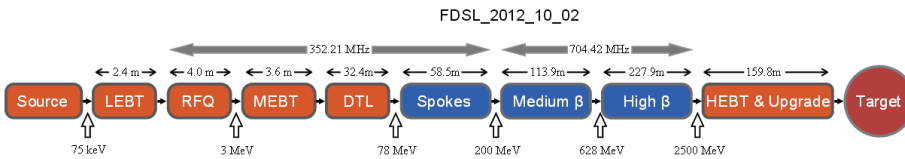


**Figure 2.1:** A block diagram of the accelerator [5]

## 2.3 Cavity and Basic Parameters

To make the cavities accelerate the protons an RF-pulse with a specific amplitude and length is applied to the cavities. When the RF-pulse is sent into the cavity it creates a standing wave that induces an electric field in the cavity. The cavity line is designed so that it takes the same time for the protons to travel from cavity to cavity as it takes for the standing wave to switch from maximum to minimum electric field. When the proton comes into the cavity it feels this electric field and gains energy from it. This results in that the proton speed is increased. The system is designed so that the protons arrive to the cavity when the field is at approximate half the maximum achievable magnitude, see point a in figure 2.2, but this is not the case for all protons. If a proton have too high speed it arrives to the cavity a little bit early and thus the fields magnitude is lower than half the maximum, see point b in figure 2.2. This results in that the proton does not gain as much energy and the speed is not increased very much. This means that the proton will arrive to the next cavity a little later than before and therefore feel a larger field, see point c in figure 2.2, closer to the designed value. The opposite happens if a proton arrives to the cavity late, then the field is higher than half maximum, which results in a higher energy gain for the proton. Now it will arrive earlier to the next cavity and therefore feel a field closer to the designed value.

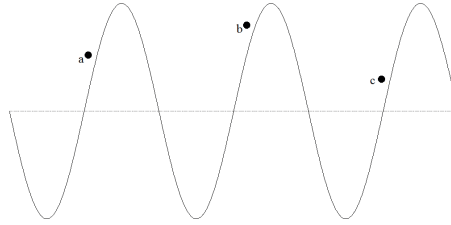


**Figure 2.2:** Graph of the standing wave [2].

### 2.3.1 Cavity Voltage

$V_{cav}$  is the absolute value of the line integral of the electric field seen by the beam along the accelerating axis, which reflects the maximum achievable energy gain for beam acceleration. It becomes a function of beam velocity factor  $\beta$  in proton acceleration. [14]

$$V_{cav} = \int_{-L/2}^{L/2} E_z(z, t) e^{i\omega z/c} dz$$

### 2.3.2 Loaded Q-value, $Q_L$

A measure of a resonant circuits ability to store energy is called the quality factor,  $Q$ , and is defined as

$$Q = 2\pi \frac{\text{stored energy in cavity}}{\text{dissipated energy per cycle}} = \frac{\omega_0 W}{P_{diss}}$$

where  $W$  is the stored energy,  $\omega_0$  is the resonance frequency and  $P_{diss}$  is the dissipated power. Assuming there are only losses in the walls of the cavity, caused by RF surface resistance, the quality factor is unloaded,  $Q_0$ . Using basic formulas from circuit theory and modelling the cavity as a resonant circuit, see figure 2.3,  $P_{diss} = \frac{V_0^2}{2R}$  and  $W = 1/2 CV_0^2$ , it can be written as

$$Q_0 = \frac{2\pi \frac{1}{2} CV_0^2}{T \frac{1}{2} \frac{V_0^2}{R}} = \frac{2\pi CR}{T}$$

where  $T$  is the time of one period of the RF-signal and  $V_0$  is the peak amplitude of the signal.

$$Q_0 = R\omega_0 C = \frac{R}{\omega_0 L} = \frac{\omega_0 W}{P_{diss}}$$

However, if the cavity is connected to something, the energy does not only dissipate in the cavity walls, it also dissipates in the external load. The external quality factor is defined as

$$Q_{ext} = \frac{\omega_0 W}{P_{ext}}$$

This gives

$$Q_L = \frac{\omega_0 W}{P_{tot}}$$

with  $P_{tot} = P_{diss} + P_{ext}$ . This means that

$$Q_L = \frac{1}{\frac{1}{Q_0} + \frac{1}{Q_{ext}}}$$

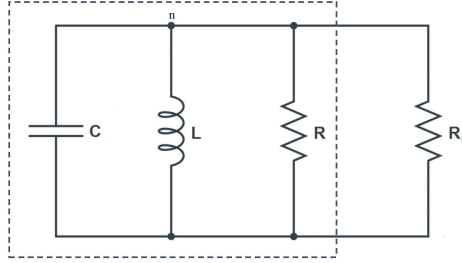


**Figure 2.3:** LCR model of the cavity, in the dashed rectangle, with an external load,  $R_L$ , connected. [1]

### 2.3.3 Beam Phase

The beam phase  $\phi_b$  is, for a given particle traversing the cavity, the phase shift from the RF phase at which it obtains the maximum energy gain. It is equivalent to the phase angle between beam and accelerating voltage in vector diagram. One typical definition of  $\phi_b$  is [17]

$$\phi_b = \arctan \left[ \frac{\int_{S_0}^{S_0+L} qE_z(s) \cdot \sin(\phi(s)) ds}{\int_{S_0}^{S_0+L} qE_z(s) \cdot \cos(\phi(s)) ds} \right]$$

where  $\phi(s)$  is the RF phase when the particle is at the coordinate  $s$  and  $L$  is the length of the cavity.

### 2.3.4 R/Q

$R/Q$  relates the stored energy and the maximum accelerating voltage acting on the beam, which only depends on the cavity shape for a given resonant mode. It measures how effective the beam-cavity energy exchange is and in proton acceleration is dependent on the beam velocity factor  $\beta$  through the relation

$$\frac{R}{Q} = \frac{|V|^2}{2\omega V}$$

### 2.3.5 Dynamic Detuning

The detuning is the difference in frequency of the RF pulse and resonance frequency of the cavity,  $\Delta\omega = \omega - \omega_0$  where  $\omega$  is the RF pulse frequency and  $\omega_0$  is the resonant frequency

of the cavity. This difference originates from that the fields created by the RF pulse is deforming the cavity causing the resonant frequency to change. Due to that the RF pulse is long,  $\sim 3.5$  ms, and the gradient level is high, the detuning becomes a key parameter in superconducting cavities. The dynamic detuning includes both the static initial detuning to compensate beam synchronous phase operation and the detuning variation during long RF pulse induced by Lorentz forces.

## 2.4 High Precision Measurement

There are many challenges to the control of the cavities and the operation methods in ESS. This is caused by the long RF pulse, almost 3 times longer than SNS and DESY, which are facilities similar to the ESS, the high beam intensity, the high beam power, the high gradient and the uncertainties in spoke cavities. For example the method of compensating the Lorentz force detuning with driving the piezo tuner by a simple half-cycle sinusoid pulse is not certain to function as desired due to the long RF pulse. Another example is that the higher beam intensity will make the beam loading heavier. The same setting error at SNS (up to  $2^\circ$  in phase and 2 % in amplitude) might not be suitable for ESS since ESS has higher beam power which leads to larger beam loss at high power linac of 5MW. ESS is the first large linac to use spoke cavities, which means that there is not very much experience with the functionality, thus creating the need for a more flexible scheme so that changes to the settings is more easily done and unexpected consequences can be avoided. There is a high energy efficiency requirement on the ESS, i.e. the energy consumption should be as low as possible. To reach this goal the power overhead required for controlling the cavity field should be minimized. The aim is to reduce the power overhead from 30 % to 10 %. It will be essential with magnitude and phase compensation at ESS. This compensation requires adequate and accurate measurements to implement. It is also important to create schemes of fast recovery in case some part of the accelerator fails.

To address the challenges at ESS, an extensive investigation of methods and novel ideas implemented or proposed in other labs are made. These methods/ideas become possible as a consequence of advances in modern technologies (flexible FPGA, faster CPU, bigger memory, and faster communication speed), novel measuring techniques, accurate system modelling, and advanced control concepts. Those possible implementations are essential to a better understanding, and thus a better operation of ESS cavity especially SRF (Superconducting Resonance Frequency) cavities.

All these concepts rely on high precision measurement of basic cavity parameters and consequent high quality data with high resolution.





# High Precision Measurement Modelling and Investigation

## 3.1 Basic Models

### 3.1.1 Cavity Model

To simulate how the cavity will behave when a RF-signal is applied MATLAB is used, or more specifically Simulink. To make a model in Simulink a mathematical description of the cavity must be used. To do this the equation from Schilcher's doctoral thesis is used [1] (equation 3.49 on page 50)

$$\frac{d}{dt} \begin{pmatrix} V_r \\ V_i \end{pmatrix} = \begin{pmatrix} -\omega_{1/2} & -\Delta\omega \\ \Delta\omega & -\omega_{1/2} \end{pmatrix} \begin{pmatrix} V_r \\ V_i \end{pmatrix} + \begin{pmatrix} R_L\omega_{1/2} & 0 \\ 0 & R_L\omega_{1/2} \end{pmatrix} \begin{pmatrix} I_r \\ I_i \end{pmatrix} \quad (3.1)$$

where  $\omega_{1/2}$  is the half 3 dB bandwidth of the cavity,  $\Delta\omega$  is the dynamic detuning and  $R_L$  is the external load.  $V_r$  and  $V_i$  are the real and imaginary part of the cavity voltage, and  $I_r$  and  $I_i$  are the real and imaginary part of the driving current. This equation is derived from Kirchoff's current law by assuming that the cavity together with the external load is a driven LCR circuit, see figure 2.3 and adding the currents in the node n, derivation over time, and rewriting the currents to get the equation dependent on the cavity voltage instead. To make the model easier to implement in Simulink the equation needs to be rewritten and divided in one real and one imaginary part. The rewriting of the real part looks like this

$$\frac{dV_r}{dt} = -\omega_{1/2}V_r - \Delta\omega V_i + R_L\omega_{1/2}I_r \quad (3.2)$$

$$\frac{dV_r}{dt} = \frac{V_{r,n+1} - V_{r,n}}{\Delta t} = -\omega_{1/2}V_{r,n} - \Delta\omega V_{i,n} + R_L\omega_{1/2}I_{r,n}$$

$$V_{r,n+1} - V_{r,n} = \Delta t(-\omega_{1/2}V_{r,n} - \Delta\omega V_{i,n} + R_L\omega_{1/2}I_{r,n})$$

$$V_{r,n+1} = V_{r,n} - \Delta t\omega_{1/2}V_{r,n} - \Delta t\Delta\omega V_{i,n} + \Delta tR_L\omega_{1/2}I_{r,n}$$

$$V_{r,n+1} = V_{r,n}(1 - \Delta t\omega_{1/2}) - \Delta t\Delta\omega V_{i,n} + \Delta tR_L\omega_{1/2}I_{r,n} \quad (3.3)$$

with  $R_L = \frac{1}{2} \left( \frac{R}{Q} \right) Q_L$  and  $\omega_{1/2} = \frac{\omega}{2Q_L}$ .

The equation for the imaginary part is almost the same

$$V_{i,n+1} = V_{i,n}(1 - \Delta t \omega_{1/2}) + \Delta t \Delta \omega V_{r,n} + \Delta t R_L \omega_{1/2} I_{i,n} \quad (3.4)$$

Using these equations the model in figure A.1 in Appendix A is made. In the model Cavity\_I is the real part of the cavity voltage and Cavity\_Q is the imaginary part.

### 3.1.2 Lorentz Force Detuning Model

The RF-signal creates an electromagnetic field, and the higher the electromagnetic field, the higher the energy that can be transferred to the protons. The drawback is that a high electromagnetic field causes strong Lorentz forces on the walls of the cavity. This causes the cavity to be deformed, and that makes the resonance frequency shift. The difference between the new resonance frequency and the applied RF-frequency can be calculated with the equation [1]

$$\Delta f = f_0 \cdot \frac{\int_{\Delta V} (\epsilon_0 E^2 - \mu_0 H^2) dV}{\int_V (\epsilon_0 E^2 + \mu_0 H^2) dV} \quad (3.5)$$

The frequency difference is changing over time, which can be described by the equation [1]

$$\frac{d}{dt} \Delta \omega(t) = -\frac{1}{\tau_m} \Delta \omega(t) - \frac{2\pi K}{\tau_m} \cdot E_{acc}^2(t) \quad (3.6)$$

with  $\Delta \omega(t) = \omega_0(t) - \omega$ . To be able to make a model in Simulink it has to be rewritten using that

$$\begin{aligned} \frac{d}{dt} \Delta \omega(t) &= \frac{\Delta \omega(t)_{n+1} - \Delta \omega(t)_n}{\Delta t} \Rightarrow \\ \Rightarrow \frac{\Delta \omega(t)_{n+1} - \Delta \omega(t)_n}{\Delta t} &= -\frac{1}{\tau_m} \Delta \omega(t)_n - \frac{2\pi K}{\tau_m} \cdot E_{acc}^2(t) \Rightarrow \\ \Rightarrow \Delta \omega(t)_{n+1} &= \left(1 - \frac{\Delta t}{\tau_m}\right) \cdot \Delta \omega(t)_n - \frac{2\pi K \Delta t}{\tau_m} \cdot E_{acc}^2(t) \end{aligned} \quad (3.7)$$

### 3.1.3 Directional Coupler Model

To measure the power used in the cavity a directional coupler is used. It can measure the forward and reflected power when the pulse is sent to the cavity. The figure of merit for the directional couplers ability to separate what is the forward and reflected power is the directivity  $D$  which is defined as  $D = S_{31} + S_{21} - S_{32}$  [9], where  $S_{31}$  is the coupling ratio, i.e. how much power of the signal is extracted,  $S_{21}$  is the insertion loss, i.e. the loss of power from the transition between the coupler and the transmission line and  $S_{32}$  is the isolation. All these terms are defined in dB.

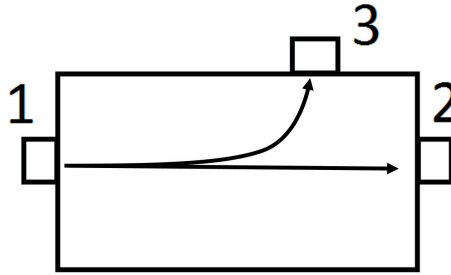


**Figure 3.1:** Directional coupler.

To demonstrate how the directivity affects the measurements, an unknown load is connected to the output, port 2 in figure 3.2, of the directional coupler. Since the load probably is not matched to the input load connected to the input, port 1, there will be a reflected signal that has an arbitrary phase. When measuring the forward voltage just a fraction of the voltage will be measured to have as little effect on the system as possible. This fraction is determined by the coupling factor. When measuring there will be a little addition from the reflected voltage. It is here the directivity has its impact. The higher directivity the less reflected voltage "leaks" into the measurement. This is because the measured voltage is described by the equation

$$V_{for}^* = 10^{-C/20} \cdot (V_{for} + 10^{-D/20} \cdot V_{ref}) \quad (3.8)$$

where  $C$  is the coupling factor and  $D$  is the directivity,  $V_{for}^*$  is the measured forward voltage. i.e. the voltage measured in port 3,  $V_{for}$  is the actual forward voltage and  $V_{ref}$  is the actual reflected voltage.

To see the effects of the directivity on the cavity measurements, a model of a directional coupler is added to the simulation. This implements equation 3.8 and the model can be seen in figure 3.2, where  $C$  is  $10^{-D/20} \cdot 10^{-C/20}$  and  $C1$  is  $10^{-C/20}$ .

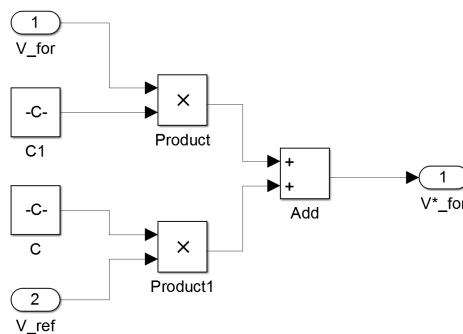


**Figure 3.2:** Model of the directional coupler in Simulink

### 3.1.4 Feedforward Control Model

The FF control model can be seen in figure 3.3, the principal is to measure the detuning information from cavity system, and in the meantime generate the required feedforward signal by equation 3.9, done in the "FF learning" block in figure 3.3, and then apply this generated FF signal to the next pulse. This model can compensate dynamic Lorentz force detuning and also static pre-detuning.

The cavity voltage can be described as [3]

$$\mathbf{V}_{\text{cav}} = \frac{R_L}{1 - i \tan \phi_D} \cdot \mathbf{I}_{\text{total}}$$

where  $\mathbf{I}_{\text{total}} = \mathbf{I}_g - \mathbf{I}_b$ ,  $R_L$  is the load resistance and  $\tan \phi_D = Q_L(\frac{\omega_0}{\omega} - \frac{\omega}{\omega_0})$  which is dependent on the detuning. The cavity voltage is taken as reference, i.e.  $\mathbf{V}_{\text{cav}} = V_{\text{cav}} + i \cdot 0$ , and writing the current in complex form gives [3]

$$V_{\text{cav}} = \frac{R_L}{1 - i \tan \phi_D} \cdot (I_{gr} - I_{br} + i(I_{gi} - I_{bi}))$$

where  $I_{gr}$  and  $I_{br}$  is the real and imaginary part of the generator current, and  $I_{gi}$  and  $I_{bi}$  is the real and imaginary part of the beam current. Using

$$\begin{aligned} I_{br} &= I_b \cos \phi_b \\ I_{bi} &= I_b \sin \phi_b \end{aligned}$$

this gives

$$\begin{aligned} (1 - i \tan \phi_D) \cdot V_{\text{cav}} &= R_L \cdot (I_{gr} - I_{br} + i(I_{gi} - I_{bi})) \Rightarrow \\ \Rightarrow \begin{cases} I_{gr} = \frac{V_{\text{cav}}}{R_L} + I_b \cos \phi_b \\ I_{gi} = -\frac{V_{\text{cav}}}{R_L} \tan \phi_D - I_b \sin \phi_b \end{cases} \end{aligned} \quad (3.9)$$

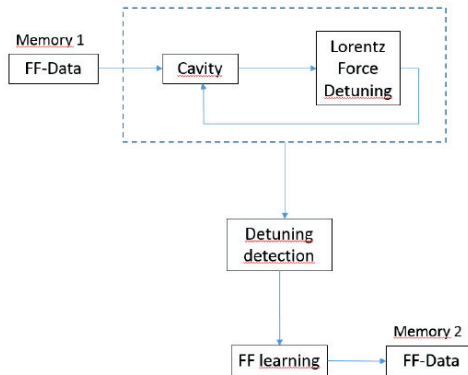


**Figure 3.3:** Feedforward model

## 3.2 Get Constant Field using only Feedforward

There are many challenges to face in the development of the ESS. One is to improve the Low Level Radio Frequency (LLRF) control. The traditional LLRF control does not work because in ESS there is a long pulse, the detuning compensation may not be adequate and the higher beam intensity lead to a heavier beam loading. One requirement of the ESS is a low energy consumption. Traditional LLRF control is using feedback to achieve a constant field in the cavities. The problem with this is that it consumes excessive energy and this is a problem in ESS. A more energy efficient method is using feedforward. This result in a field that is almost constant and to get it completely constant feedback can be used, but since the error is small it do not need as much energy.

Feedforward is a good control method to reduce the effect of perturbations that do not change between different runs. [10] The feedforward used in the simulations in this thesis consists of the generator current calculated using the detuning of the cavity since it does not change very much between pulses if the input is the same. Therefore the ideal generator current can be calculated, thus determining the feedforward table.

To simulate, all the necessary parameters are calculated, i.e. the optimal Q-value of the cavity,  $Q_{L,opt}$ , the measure of how effectively the cavity can create a accelerating voltage,  $(\frac{R}{Q})$ , the cavity voltage,  $V_{cav}$ , the beam current,  $I_b$ , the phase of the beam,  $\phi_b$ , the injection time,  $t_{inj}$  and the pre-detuning,  $\Delta f$ .  $(\frac{R}{Q})$ ,  $V_{cav}$  and  $I_b$  are already known. To calculate the other ones equation 3.9 and the following equations are used [3]

$$R_L = \frac{1}{2} \left( \frac{R}{Q} \right) Q_L$$

$$\tan\phi_D = Q_L \left( \frac{\omega_0}{\omega} - \frac{\omega}{\omega_0} \right)$$

**Table 3.1:** Parameters used in the simulations.

$V_{cav}$	$Q_L$	$R/Q$	$I_b$	sync phase	$t_{inj}$	pre-detuning
5.7MV	$2.478 \cdot 10^5$	397 $\Omega$	62.5mA	-22°	155.2 $\mu$ s	287.2Hz

### 3.2.1 $Q_L$ Optimization

To calculate this the imaginary part of  $\mathbf{I}_g$  in equation 3.9 is set to 0 and the equation [3] becomes:

$$P_g = \frac{1}{8} |\mathbf{I}_g|^2 R_L \Rightarrow$$

$$\begin{aligned} P_g &= \frac{1}{8} I_{gr}^2 R_L = \frac{1}{8} R_L \left( \frac{V_{cav}}{R_L} + I_b \cos\phi_b \right)^2 = \frac{1}{8} R_L \left( \frac{V_{cav}^2}{R_L^2} + 2 \frac{V_{cav}}{R_L} I_b \cos\phi_b + I_b^2 \cos^2\phi_b \right) = \\ &= \frac{V_{cav}^2}{8R_L} + \frac{V_{cav}}{8} I_b \cos\phi_b + R_L I_b^2 \cos^2\phi_b \end{aligned}$$

Then to get the minimum power consumption, the derivative of the equation is taken

$$P'_g(R_L) = -\frac{V_{cav}^2}{8R_L^2} + 0 + \frac{I_b^2 \cos^2 \phi_b}{8}$$

Rearranging and using that  $R_L = \frac{1}{2} \left( \frac{R}{Q} \right) Q_L$  and at minimum  $P'_g(Q_{L,opt}) = 0$  where  $Q_{L,opt}$  is the Q-value when the power consumption is as low as possible.

$$\begin{aligned} Q_{L,opt}^2 &= \frac{V_{cav}^2}{\left(\frac{1}{2}\right)^2 \left(\frac{R}{Q}\right)^2 I_b^2 \cos^2 \phi_b} \Rightarrow \\ Q_{L,opt} &= \frac{V_{cav}}{\left(\frac{1}{2}\right) \left(\frac{R}{Q}\right) I_b \cos \phi_b} \end{aligned} \quad (3.10)$$

### 3.2.2 Pre-Detuning Optimization

To counteract the detuning in the beginning, the cavity is pre-detuned by applying a signal with the pre-detuning frequency calculated with the equation [3]

$$\tan \phi_D = Q_L \left( \frac{\omega_0}{\omega} - \frac{\omega}{\omega_0} \right) = Q_L \left( \frac{\omega_0^2 - \omega^2}{\omega_0 \omega} \right) = Q_L \left( \frac{(\omega_0 + \omega)(\omega_0 - \omega)}{\omega_0 \omega} \right) \quad (3.11)$$

Since the working frequency is close to the resonance frequency,  $\omega \approx \omega_0$ , and  $\omega_0 - \omega = \Delta\omega$ , the equation can be simplified to

$$\begin{aligned} \tan \phi_D &= Q_L \frac{2\omega_0 \Delta\omega}{\omega_0 \omega_0} = Q_L \frac{2\Delta\omega}{\omega_0} = [\omega = 2\pi f] = \frac{2Q_L}{f_0} \cdot \Delta f \Rightarrow \Delta f = \frac{\tan \phi_D f_0}{2Q_L} = \\ &= [\tan \phi_D = -\tan \phi_b] \Rightarrow \Delta f = -\frac{f_0 \tan \phi_b}{2Q_L} \end{aligned} \quad (3.12)$$

### 3.2.3 Injection Time Optimization

To get the injection time,  $t_{inj}$ , this equation is used [3]

$$V_{cav} = I_g R_L (1 - e^{-\frac{t_{inj}}{\tau}}) \Leftrightarrow e^{-\frac{t_{inj}}{\tau}} = 1 - \frac{V_{cav}}{I_g R_L} = \frac{I_g R_L - V_{cav}}{I_g R_L}$$

assuming that the generator current is constant during the injection time. Since the power consumption still is to be minimized,  $I_{gi} = 0 \Rightarrow I_g = I_{gr}$

$$\begin{aligned} -\frac{t_{inj}}{\tau} &= \ln \left( \frac{I_{gr} - \frac{V_{cav}}{R_L}}{I_{gr}} \right) = \ln \left( \frac{\frac{V_{cav}}{R_L} + I_b \cos \phi_b - \frac{V_{cav}}{R_L}}{I_{gr}} \right) \Leftrightarrow \\ &\Leftrightarrow t_{inj} = \tau \ln \left( \frac{I_{gr}}{I_b \cos \phi_b} \right) \end{aligned} \quad (3.13)$$

### 3.2.4 Frequency Tracking During Filling Time

When the cavity is turned on the cavity RMS voltage rises gradually. This is called the filling of the cavity. During the time it takes to fill it, the pre-detuning keeps working, but since there is no beam through the cavity there is no compensation for the pre-detuning. This leads to a perturbation of the steady state, shown on the left hand side of figure 3.4. So called frequency tracking is an effective method to avoid this. The method consists of modulating the phase of the input with the equation

$$\phi = \int \Delta\omega dt \quad (3.14)$$

The cavity amplitude is still the same, but the cavity phase is increasing during the whole filling time. But to make this work, a proper phase offset has to be applied to get the right phase at the end of the injection time.

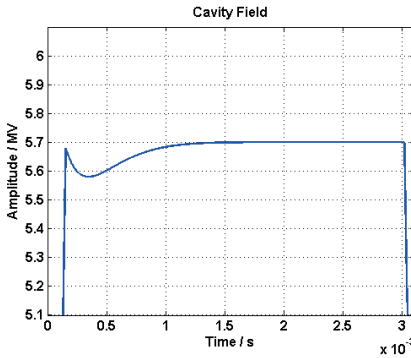


Figure 3.4: Amplitude

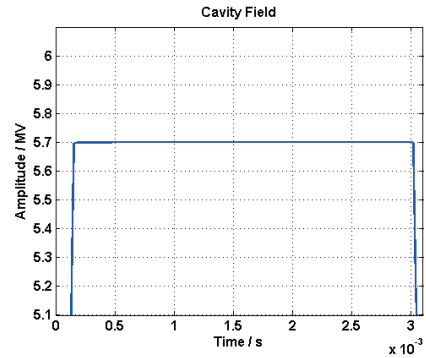
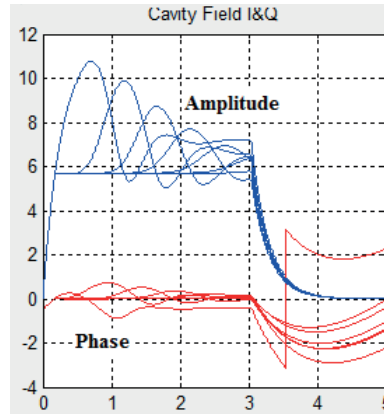


Figure 3.5: Amplitude

### 3.2.5 Lorentz Force Detuning Compensation

Lorentz force detuning compensation is made according to the feedforward model in section 3.1.4. The feedforward signal acquired from the previous pulse is applied to the current pulse to compensate for the dynamic detuning caused by Lorentz force induced mechanical excitation. Only one iteration is required if the detuning information for feedforward learning is derived from a constant cavity field. If that is not the case, more iterations are required to get a constant cavity field, as shown in figure 3.6. An alternative way giving fewer iterative steps is to measure the detuning information correctly in advance and apply this information to the feedforward table in operation.





**Figure 3.6:** The amplitude and phase) of the iterated cavity field

### 3.3 Gradient Ramp-up Procedures

#### 3.3.1 General Procedures

When turning on the cavity it takes some runs to calibrate the feedforward and the control system. This uses a lot of energy if using the desired end gradient, and to minimize this a ramp-up of the cavity gradient is performed. This gradient is controlling the generator current and while ramping up the gradient many characteristics of the cavity can be determined, e.g. detuning, injection time and loaded Q-value.

To simulate the gradient ramp up a simulation series was started. The cavity gradient was increased in steps of 0.1 between the simulations, starting at 0.1 going to 1. The result can be seen in figure 3.7. As can be seen it is quite good for lower gradients, but for higher gradients the field starts to diverge from the desired constant field, both in amplitude and phase.

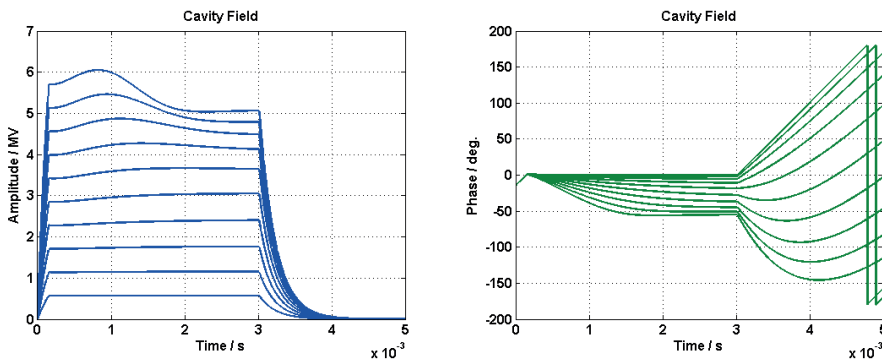


**Figure 3.7:** The amplitude and phase of the cavity field when just increasing the scaling factor from 0.1 to 1 and the detuning constant  $K=30$  Hz/MV

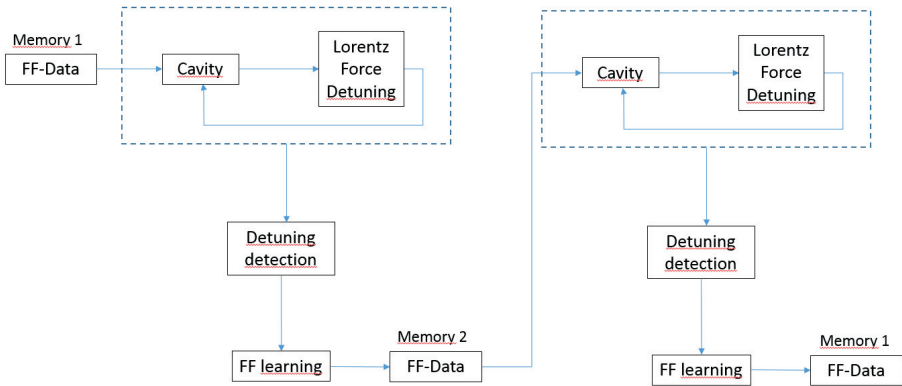


**Figure 3.8:** The iterative loop to acquire a good cavity gradient ramp-up.

### 3.3.2 Ramp-up with Different Feedforward Strategies

To improve the field a second simulation at every gradient is added using the feedforward table acquired from the first simulation with that gradient, see figure 3.8. The result can be seen in figure 3.9 and already the field has improved quite a bit. Now it is only for the high gradients that the amplitude is diverging from the wanted straight lines, but the phases are almost constant at zero during the pulse.

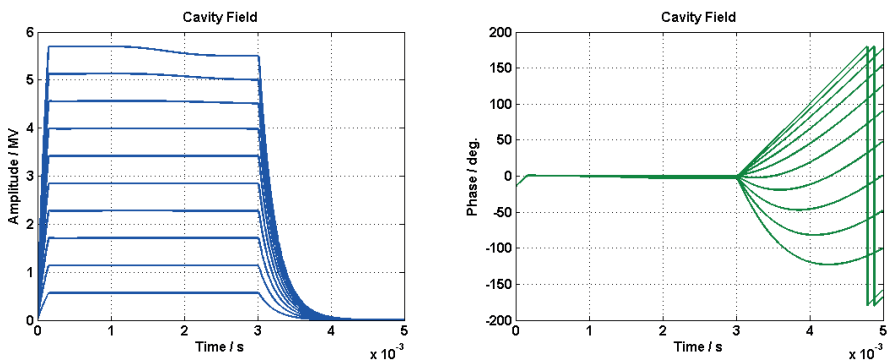


**Figure 3.9:** The amplitude and phase of the cavity field with the feedforward table from the previous scaling factor when increasing the scaling factor from 0.1 to 1 and the detuning constant  $K=30$  Hz/MV

To get the wanted result it takes three iterations and the result can be seen in figure 3.10. Now the amplitude diverges at most 0.35 % and the phase diverges at most  $0.5^\circ$ .

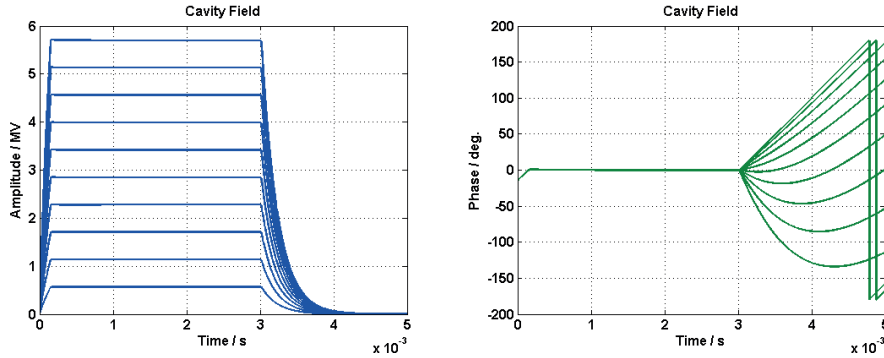


**Figure 3.10:** The amplitude and phase of the cavity field after three iterations of the feedforward table has been done, increasing the scaling factor from 0.1 to 1 and the detuning constant  $K=30$  Hz/MV

## 3.4 Effects of Inaccurate Parameters on Ramp-up Procedures/Feedforward

### 3.4.1 Inaccurate Cavity Voltage

The inaccuracy of the cavity voltage refers to the deviation of the real setting point to the design value. The design value is the real necessary amplitude required by the beam. The value depends on the calibration method, a 2 % error or even higher could be expected in the high energy part using phase scan (beam based calibration), while a 5 % error or even larger could be expected if only RF based calibration of the cavity voltage is used.

The influence of inaccurate cavity voltage leads to the the previously optimized parameters like  $Q_L$ ,  $t_{inj}$  and pre-detuning to no longer be optimal. Re-adjustment has to be done in order to get a constant field. The adjustment resolution of pre-detuning and injection time determines how good the field flatness can become.

**Table 3.2:** Effect of inaccurate cavity voltage on important parameters.

Error	$Q_L$	$t_{inj}$ ( $\mu s$ )	pre-detuning (Hz)
5 %	2.6015	160.7	273.5
2 %	2.5272	157.4	281.5
1 %	2.5024	156.3	284.3
0 %	2.4776	155.2	287.2

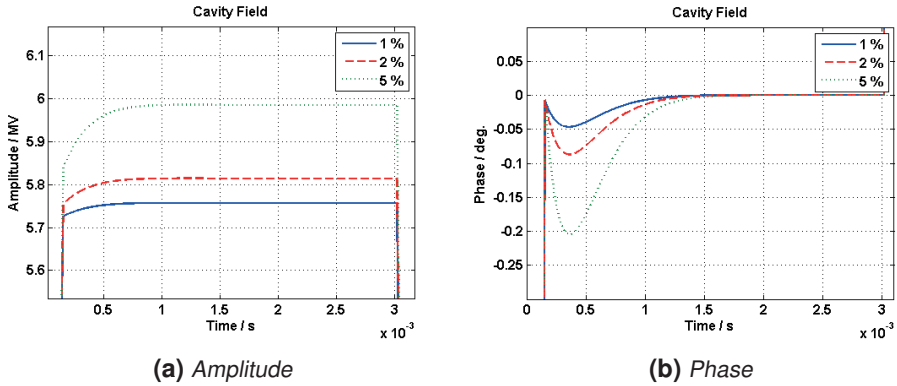


**Figure 3.11:** Effect of voltage errors on the amplitude and phase of the cavity field.

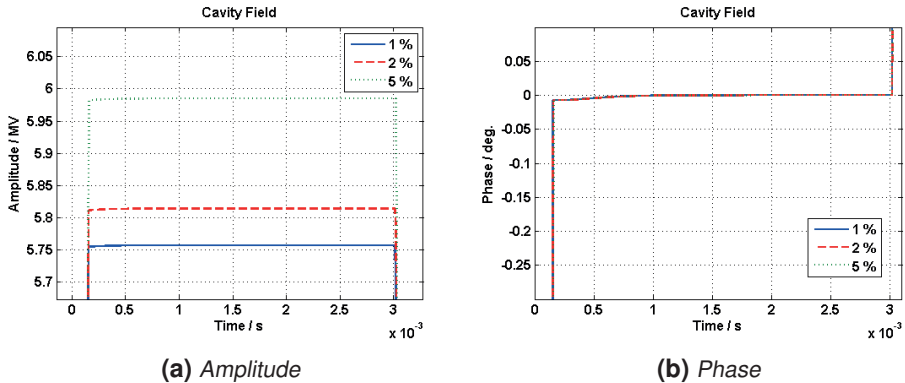


**Figure 3.12:** Effect of voltage errors on the amplitude and phase of the cavity field after acquiring and using a new feedforward table.

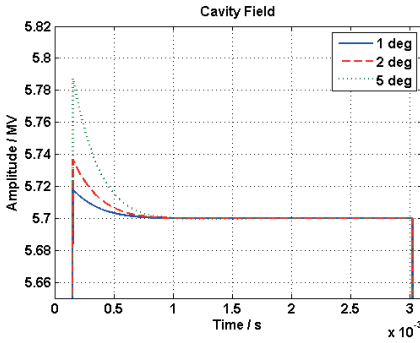
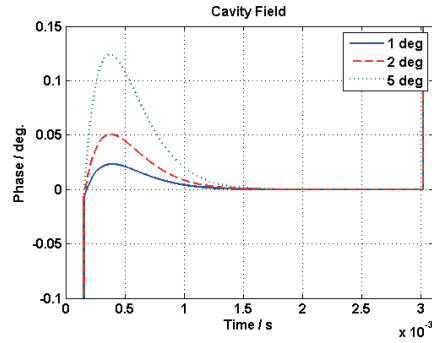
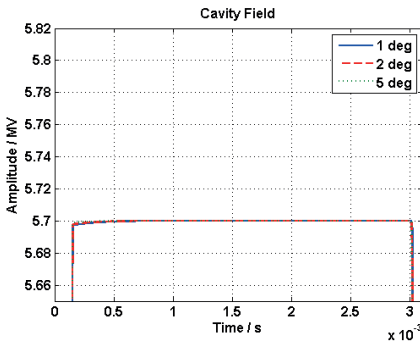
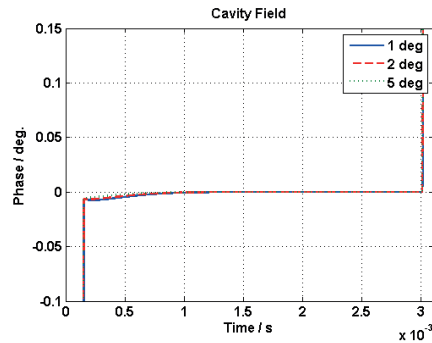
### 3.4.2 Inaccurate Synchronous Phase

As can be seen in figure 3.13 an incorrect synchronous phase has a larger impact on the amplitude of the cavity field than the phase of the field. Even with a  $5^\circ$  error the phase does not diverge more than  $0.13^\circ$  from the ideal value of zero. At the same time the amplitude diverges almost 1.5 % from the ideal flat field.

In figure 3.14 simulations with the incorrect synchronous phase and the corresponding injection time and pre-detuning calculated with Equations 3.12 and 3.13 have been done. A new feedforward table has also been acquired using these parameters. The result is that the amplitude is almost constant, within 0.1 % of the ideal flat field and the phase is within  $0.01^\circ$ .

**Table 3.3:** Effect of inaccurate phase on important parameters.

Error	$Q_L$	$t_{inj}$ ( $\mu s$ )	pre-detuning (Hz)
5 °	2.4022	151.8	224.1
2 °	2.4447	153.7	262.2
1 °	2.4607	154.4	274.7
0 °	2.4776	155.2	287.2

**(a)** Amplitude**(b)** Phase**Figure 3.13:** Effect of synchronous phase errors on the amplitude and phase of the cavity field.**(a)** Amplitude**(b)** Phase**Figure 3.14:** Effect of synchronous phase errors on the amplitude and phase of the cavity field after acquiring and using a new feedforward table.

### 3.4.3 Inaccurate R/Q

An inaccurate R/Q value affects the cavity field quite much as can be seen in Figures 3.15 and 3.16. The phase is still within 0.25 degrees which is within the desired range of maximum one degree deviation. The amplitude however deviates much more. Both when the R/Q value is larger and smaller than optimum the field deviates as much as the R/Q value deviates which is not surprising since this parameter is a large part of the cavity equation, equation 3.3 and 3.4.

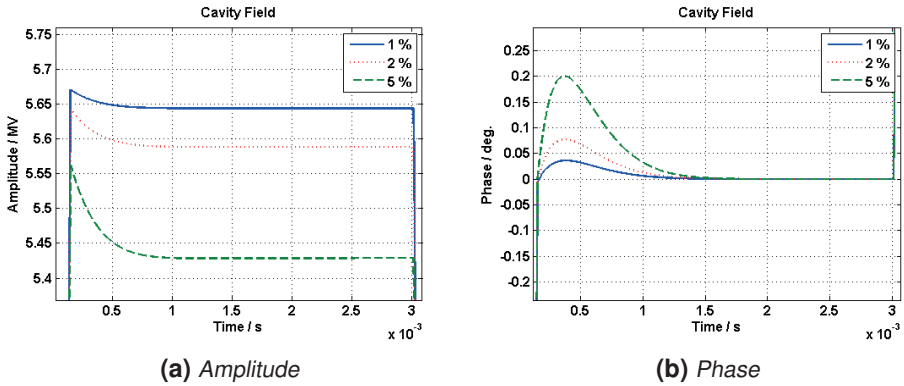


**Figure 3.15:** Effect of an R/Q value larger than the optimal on the amplitude and phase of the cavity field.

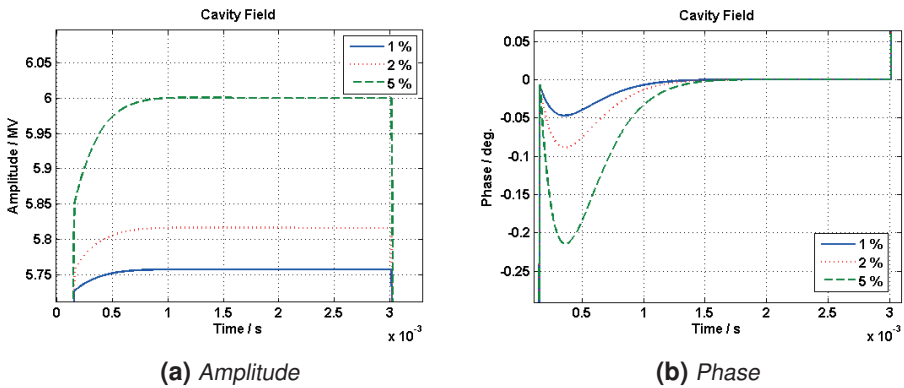


**Figure 3.16:** Effect of an R/Q value smaller than the optimal on the amplitude and phase of the cavity field.

### 3.4.4 Inaccurate Quality Factor

An inaccurate quality factor has a large effect on the cavity field, which is seen in Figures 3.17 and 3.18. The result is almost the same as when the R/Q is inaccurate, which is as expected as  $R_L = \frac{1}{2} \frac{R}{Q} Q_L$ , so if one of them deviates 1% then  $R_L$  deviates 1%. This means that a correct value of the quality factor and the R/Q is very important.

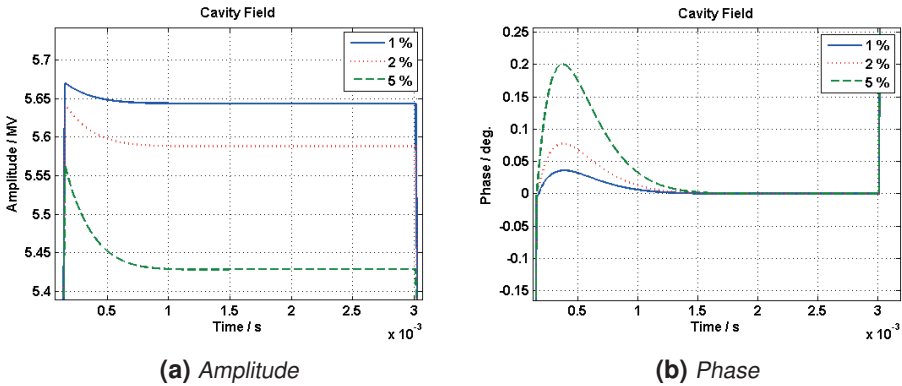


**Figure 3.17:** Effect of a  $Q_L$  value larger than the optimal on the amplitude and phase of the cavity field.

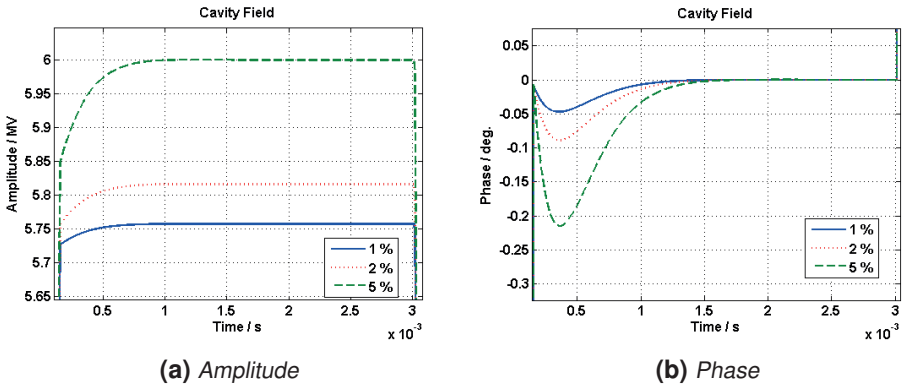


**Figure 3.18:** Effect of a  $Q_L$  value smaller than the optimal on the amplitude and phase of the cavity field.

### 3.4.5 Inaccurate Dynamic Detuning

As can be seen in figure 3.19 the dynamic detuning error has some impact on the cavity field, but since it is something that is calculated using measurements there are always some uncertainties that can not be predicted and there will be some fluctuations of the amplitude and phase. As can be seen in figure 3.19 the larger the uncertainties the larger the deviation from the optimum. It is only the 10 % plot that is outside the acceptable region of  $1^\circ$  in phase and 1 % in amplitude. This means that the method is not affected very much by the inaccuracies.

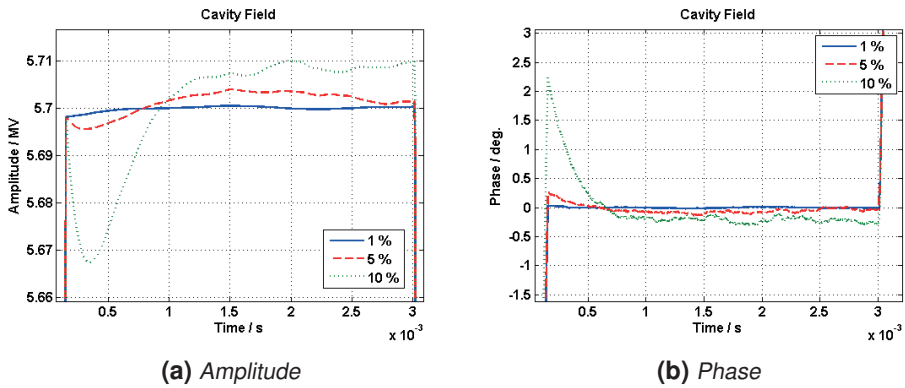


**Figure 3.19:** Effect of dynamic detuning errors on the amplitude and phase of the cavity field.

## 3.5 Improvement Investigation of Accuracy/Precision in System Modelling

### 3.5.1 Hardware Limitation

#### 3.5.1.1 Directivity of Directional Coupler

Cavity field simulations were performed using directivities of 20, 30 and 40 dB. These values cover the usual range of directivities for directional couplers. Here only feedforward and no feedback is used. In figure 3.20 the detuning plot for infinite directivity can be seen. As can be seen in figure 3.21 the higher the directivity the smaller the difference to the ideal case. This is as expected since a large directivity has a small effect on the reflected power. As shown in equation 3.8 a large  $D$  gives a small coefficient in front of  $P_{ref}$ .

The impact of different directivities, i.e. 20, 30 and 40 dB, on the cavity field amplitude and phase is plotted in figure 3.22a and 3.22b. In the ideal case the amplitude should be constant at 5.7 MV and to make it sufficiently good the amplitude should not vary more than 1%. This is not the case when the directivity is 20 dB because it diverges with approximately 0.21 MV as we can see in figure 3.22a



$$\frac{5.7 - 5.49}{5.7} = \frac{0.21}{5.7} \approx 3.68\%$$

When the directivity is 30 dB the amplitude only diverges with approximately 0.07 MV

$$\frac{5.7 - 5.63}{5.7} = \frac{0.07}{5.7} \approx 1.23\%$$

The best result is when the directivity is 40 dB, which is as suspected. Now the amplitude only diverges approximately 0.02 MV

$$\frac{5.7 - 5.68}{5.7} = \frac{0.02}{5.7} \approx 0.351\%$$

To fulfill the requirements the phase should also not diverge more than 1° from 0 during the time of the beam. As can be seen in figure 3.22b on page 24 that this requirement is fulfilled when the directivity is 30 and 40 dB. When the directivity is 20 dB however, the phase is diverging almost 3°.

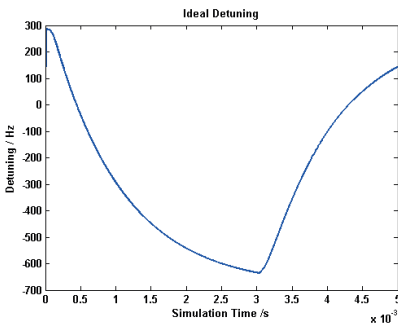


Figure 3.20: Ideal detuning for K=30

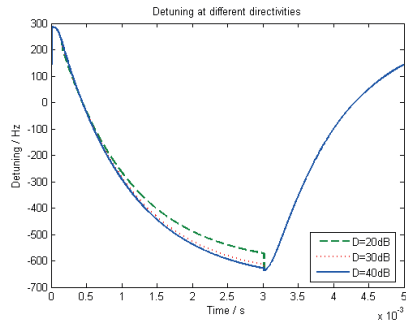
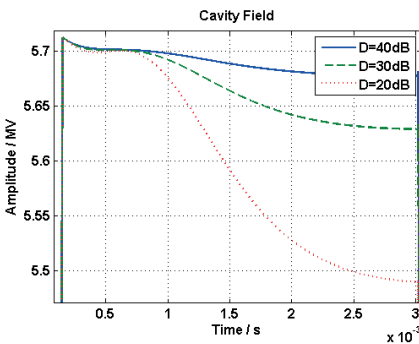
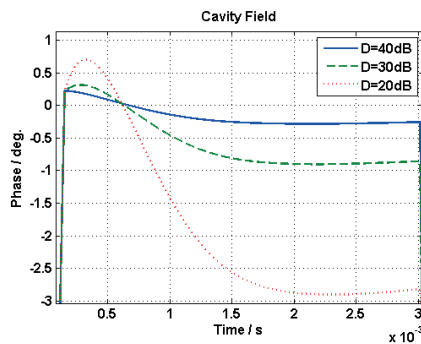


Figure 3.21: Effect of different directivities on the detuning



(a) The amplitudes.



(b) The phases.

Figure 3.22: Amplitude and phase of the cavity fields for the different directivities.

### 3.5.1.2 Coupling factor of the Directional Coupler

The coupling factor's impact on the cavity field and the detuning has also been investigated using only feedforward and no feedback. To get the proper level of the forward and reflected power from the directional coupler, the output power from the coupler needs to be amplified with a factor of  $10^{C/10}$ , where  $C$  is the coupling factor. The problem is that the coupling factor specified for the directional coupler is not always exact. For example, the coupler used in this thesis has a specified coupling factor,  $C$ , equal to 60 dB, but what if it is not 60 dB but 60.1 dB. This will lead to an extra 0.1 dB amplification, and this may affect the cavity field and the detuning since the forward power is used for calculating the detuning and to set a correct feedforward signal.

In figures 3.23 and 3.24 the result from simulations with the coupling factor equal to 60.1 and 61 dB respectively. It can be seen that the amplitude of the cavity field is getting worse the more times the feedforward is generated. As expected the error is larger if the coupling factor is 61 dB.

Looking at figure 3.23a it can be seen that, using the feedforward acquired from the first simulation (red line), the amplitude now deviates at the most approximately 0.015 MV, which is an error of approximately 0.26 % which means that it still fulfils the requirement of maximum 1 % deviation. The phase deviates  $0.24^\circ$  and so fulfils the requirement of maximum of  $1^\circ$  deviation. After another feedforward acquired (blue line) the amplitude deviates approximately 0.022 MV, which is a deviation of approximately 0.39 %, and the phase deviates  $0.31^\circ$ . This means that it still fulfils the required values.

For when the directivity is 61 dB however, the error is much larger. Already after acquiring the first feedforward table, the amplitude diverges with approximately 0.16 MV, which corresponds to an error of 2.8 %, and the phase diverges with approximately  $2.45^\circ$ . This only gets worse after acquiring the second feedforward table. Now the amplitude diverges with 0.2 MV, which corresponds to an error of 3.5 %, and the phase diverges with approximately  $3^\circ$ , well above the maximum error limit.

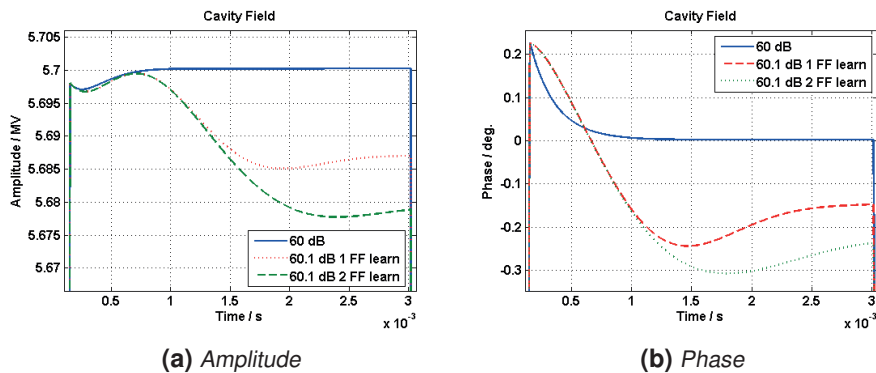


**Figure 3.23:** Effect of a coupling factor of 60.1 dB on the cavity field.

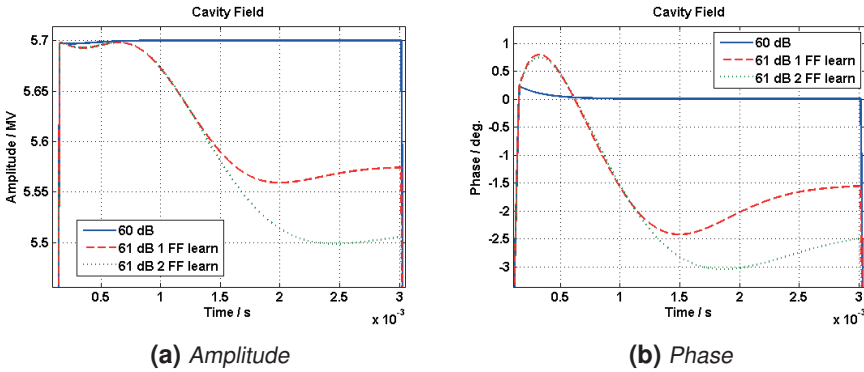


**Figure 3.24:** Effect of a coupling factor of 61 dB on the cavity field.

### 3.5.1.3 Resolution Limitation of Adjustable Injection Time and Pre-detuning

Optimized parameters like  $Q_L$ , pre-detuning and injection time are no longer optimal under calibration errors. As a result, cavity response deviates from the design value at the beginning of beam injection in feedforward mode. A big overshoot then follows when closing the feedback control loop, which is one of the reasons to keep adequate power overhead away from klystron saturation. A re-adjustment has to be made in order to get a constant field in feedforward mode by changing the pre-detuning value and the beam injection time. The adjustment resolution of pre-detuning and injection time determines how good the field flatness can be.

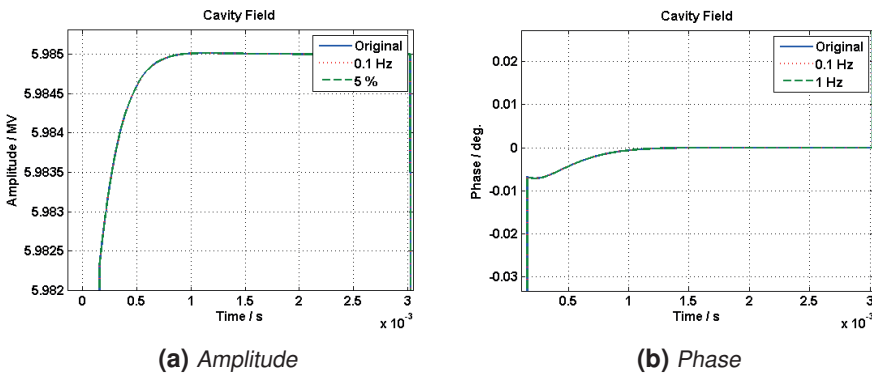


**Figure 3.25:** Effect of inaccurate pre-detuning.

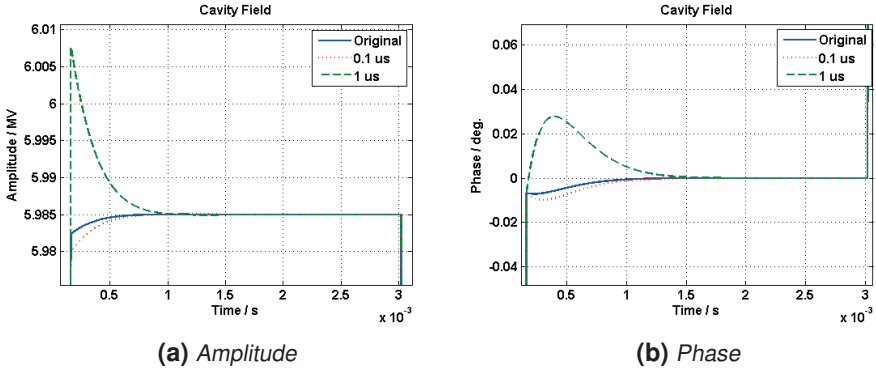


**Figure 3.26:** Effect of inaccurate injection time.

As can be seen in Figures 3.25 and 3.26 the cavity field is more dependent on a correct injection time than a correct pre-detuning. A small deviation of the pre-detuning has almost no effect on the cavity field.

## 3.5.2 Measurement Algorithm Limitation

### 3.5.2.1 Detuning

To measure the detuning during the pulse we use [1]

$$\Delta\omega = \omega_{1/2} \cdot \tan(\Delta\phi) \quad (3.15)$$

where  $\Delta\phi = \phi_{cav} - \phi_{for}$ , which is the phase difference between the cavity field and the forward power, and  $\omega_{1/2} = \frac{\omega}{2Q_L}$ . The detuning after the pulse is measured as [1]

$$\Delta\omega = \frac{d}{dt}\phi_{cav} \quad (3.16)$$

To calculate the detuning of the cavity this differential equation is used [8]

$$\frac{dV_{cav}}{dt} = -(\omega_{1/2} - i\Delta\omega(t))V_{cav} + 2\omega_{1/2}V_{for} \quad (3.17)$$

where  $V_{for}$  is the forward voltage. To calculate the detuning we rewrite the equation to

$$\Delta\omega(t) = \text{Im}\left(\frac{\frac{dV_{cav}}{dt} - 2\omega_{1/2}V_{for}}{V_{cav}}\right) \quad (3.18)$$

since  $V_{cav}$  is complex this leads to that

$$\frac{dV_{cav}}{dt} = \frac{dV_r}{dt} + i\frac{dV_i}{dt}$$

This is implemented in the model like the configuration in figure A.2 in Appendix A.

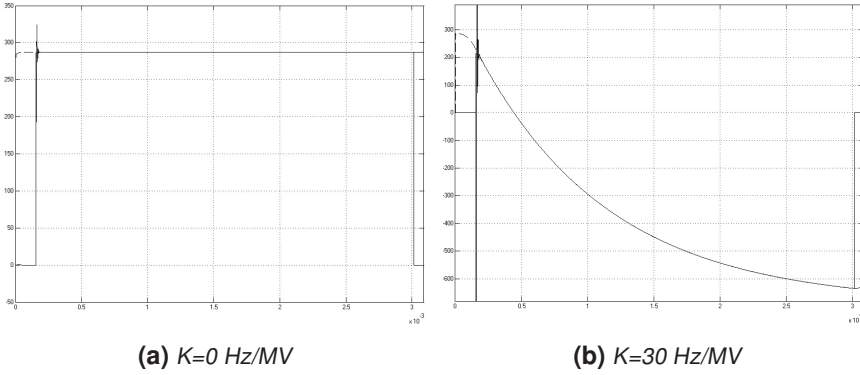


**Figure 3.27:** Detuning calculated with equation 3.15 (whole) and 3.18 (dashed)

In figure 3.27 the result of the new and old methods of calculating the detuning is shown. As can be seen they are almost identical which indicates that the new method works in the ideal case.

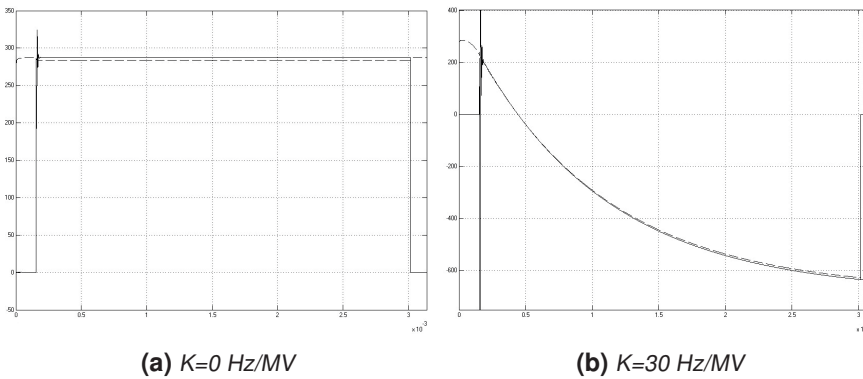


**Figure 3.28:** Detuning calculated with equation 3.15 (whole) and 3.18 (dashed) with coupling factor 60.1 dB

Figure 3.28 shows the effect of the wrong coupling factor on the detuning using the Equations 3.15 and 3.18. As can be seen the difference between the methods is small, but equation 3.15 seems to be less dependent on the coupling factor.

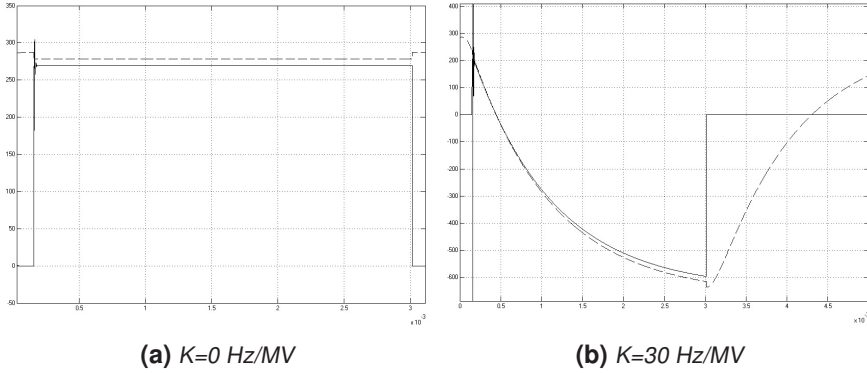


**Figure 3.29:** Detuning calculated with equation 3.15 (whole) and 3.18 (dashed) with 30 dB directivity.

As can be seen in figure 3.29 there is a small difference between the two measurement methods. When comparing figure 3.29b with the ideal detuning in figure 3.20 it looks like the method using the cavity and forward voltage is slightly closer to the truth than the method of using only the phase difference. This may depend on that the part of the reflected power that contributes to the forward power affects the phase more than the amplitude.

### 3.5.2.2 $Q_L$

The measurement method currently used for  $Q_L$  calculates the slope of the decay of the cavity voltage when the pulse is over. This is done by assuming that the decay can be described by the function

$$V_{cav} = A \cdot e^{-t/\tau} \quad (3.19)$$

where  $A$  is a constant,  $t$  is the time and  $\tau$  is the time constant. Starting with the logarithm of the cavity voltage which gives [6]

$$\ln(V_{cav}) = \ln(A) - \frac{t}{\tau}$$

This is a linear equation, i.e. on the form  $y = kx + m$ , with  $x = t$ ,  $y = \ln(V_{cav})$  and  $m = \ln(A)$ . This means that the slope,  $k$ , is  $-\frac{1}{\tau}$ . Using that  $\tau = \frac{2Q_L}{\omega_0}$  [1], the slope,  $k$ , is

$$k = -\frac{1}{\tau} = -\frac{\omega_0}{2Q_L} \Rightarrow Q_L = -\frac{\omega_0}{2k} \quad (3.20)$$

The same equation used for calculating the detuning, equation 3.18, can be used to calculate the  $Q_L$ -value since  $\omega_{1/2} = \frac{\omega_0}{2Q_L}$ . Rewriting the equation leads to

$$\omega_{1/2} = \frac{\frac{dV_{cav}}{dt} - i\Delta\omega(t) \cdot V_{cav}}{2V_{for} - V_{cav}} \quad (3.21)$$

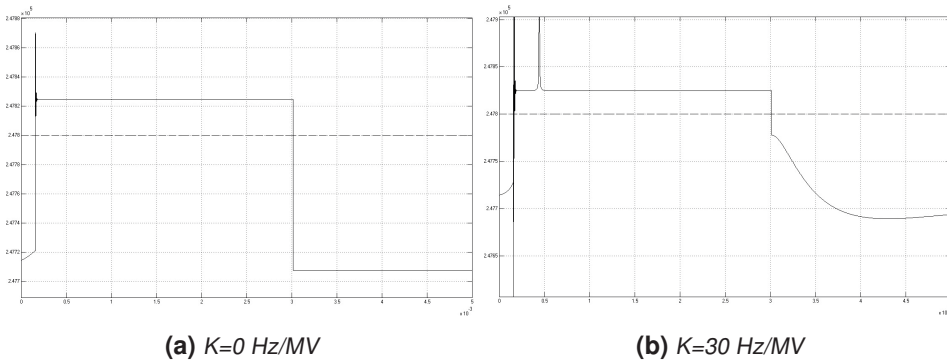


**Figure 3.30:** Loaded quality factor,  $Q_L$ , calculated with equation 3.21 (whole) and the input  $Q_L$  (dashed) with different  $K$ -values.

In figure 3.30 the result of calculations of  $Q_L$  for simulations with  $K=0$  and 30 Hz/MV. It can be seen that the value is close to the value used at the beginning of the simulation, it is not constant but within a good range of the correct value. The spike when  $K=30$  Hz/MV is probably caused by  $2V_{for}$  being close to  $V_{cav}$ . The spike could cause some problems, but it is still quite close to the correct value.

In figure 3.31 the impact of a wrong coupling factor is shown. The plot show that in the beginning the  $Q_L$ -value is quite far from the inserted value, dashed line, but at the end, after the pulse it is close. This means that this method is affected by the incorrect coupling factor, but a value close to the correct one can be achieved after the pulse. Using equation 3.20 results in the same value as when the coupling factor is correct. This means that this method is not affected by the coupling factor.

In figure 3.32 the result of calculation of the loaded quality factor,  $Q_L$ , with a directivity of 30 dB and two different  $K$  values, 0 and 30 Hz/MV. As can be seen it is not constant which makes it hard to determine the correct value. Another drawback is that it that it goes up to the value that is put into the simulation, dashed line, but when it reaches that value it instantly drops down to an incorrect value and when the pulse stops the value drops even lower. This means that this measurement method is very dependent on the directivity.

Using equation 3.20 the  $Q_L$ -value results in a value that is within 0.01% of the input value, which means that this method is not affected by the directivity.

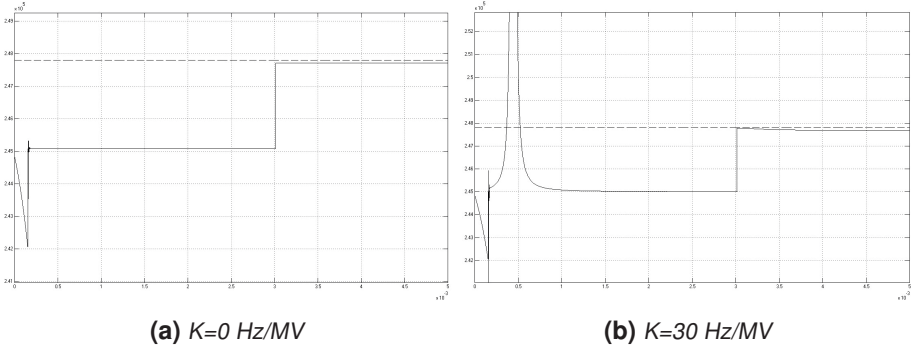


**Figure 3.31:** Loaded quality factor,  $Q_L$ , calculated with equation 3.21 (whole) and the input  $Q_L$  (dashed) with coupling factor 60.1 dB

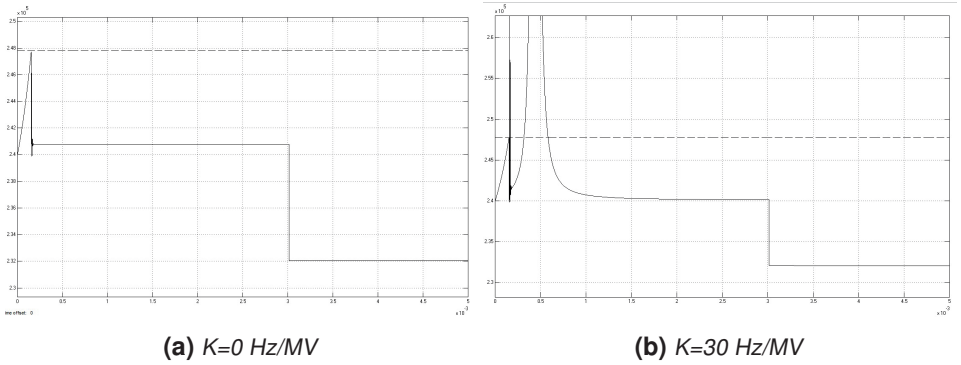


**Figure 3.32:** Loaded quality factor,  $Q_L$ , calculated with equation 3.15 (whole) and 3.18 (dashed) with 30dB directivity.

## 3.6 Other Ways of Improving the Measurements

### 3.6.1 RF Power Based Calibration for $Q_L$ and Detuning

Deriving  $Q_L$  and detuning from differential equation 3.18 seem promising to achieve high accuracy, but is limited by the forward/reflected power calibration. The measured forward power and reflected power always deviates somewhat from the real powers that goes into and are reflected from the cavity. This is due to reflection in the waveguide, the cables, the measurement devices, and system imperfection such as directivity and incorrect coupling factor. Most likely the relationship between these powers is of the first order (assuming linear cross-talk and no power cross-talk from cavity to cavity) [12];

$$\begin{aligned}
 V_{for} &= aV_{for}^* + bV_{ref}^* \\
 V_{ref} &= cV_{for}^* + dV_{ref}^* \\
 V &= V_{for} + V_{ref}
 \end{aligned}
 \tag{3.22}$$



where  $V_{for}^*$  and  $V_{ref}^*$  are the measured values and  $a$ ,  $b$ ,  $c$  and  $d$  are unknown constants.

A good power calibration is essential based on experience from other labs. In this section two power calibration methods, one in DESY and one in Fermilab, are investigated. In DESY the calibration procedure for forward and reflected wave is as follows:

1. Write equation 3.22 as  $V = XV_{for}^* + YV_{ref}^*$  with  $X = a + c$  and  $Y = b + d$ .
2. Using a single pulse with data points  $V(t_k)$ ,  $V_{for}^*(t_k)$ ,  $V_{ref}^*(t_k)$ ,  $k = 1..N$  a linear, overdetermined system of equations can be stated

$$\begin{pmatrix} V(t_1) \\ V(t_2) \\ \vdots \\ V(t_N) \end{pmatrix} = \begin{pmatrix} V_{for}^*(t_1) & V_{ref}^*(t_1) \\ V_{for}^*(t_2) & V_{ref}^*(t_2) \\ \vdots & \vdots \\ V_{for}^*(t_N) & V_{ref}^*(t_N) \end{pmatrix} \begin{pmatrix} X \\ Y \end{pmatrix} \quad (3.23)$$

$X$  and  $Y$  can now be determined using multiple linear regression.

3. A measurement when there is no forward power is done. Using  $V_{for} = aV_{for}^* + bV_{ref}^*$  gives

$$-V_{ref}^*/V_{for}^* = a/b := Z \quad (3.24)$$

4. Given  $X$ ,  $Y$ ,  $Z$  and for example  $a$  is known,  $b$ ,  $c$  and  $d$  can be calculated as follows

$$\begin{aligned} b &= \frac{a}{Z} \\ c &= X - a \\ d &= Y - \frac{a}{Z} \end{aligned} \quad (3.25)$$

5. To determine  $a$  a  $\chi^2$ -criterion of the cavity equation in polar coordinates is made. If the bandwidth is constant over the pulse, the constant  $a$  can be calculated numerically.

In Fermilab, the procedure is as below [13]

1. A relative complex gain is determined by comparing the phase and the magnitude of the reflected power in the decay region, to the probe signal in the same region. This is done with the equation:

$$G_{ref} = \frac{\langle P * P \rangle_{decay}}{\langle P * R \rangle_{decay}}$$

This gain then scales the reflected power over the entire pulse using equation:

$$R_{correct} = G_{ref} \cdot R_{raw}$$

2. A small part of the forward power,  $C_{for}$ , is contamination from the reflected power. This contamination is estimated by comparing the forward power with the reflected power in the decay region. To do this the following equation is used:

$$C_{for} = \frac{\langle F * F \rangle_{decay}}{\langle F * R \rangle_{decay}}$$

To get the correct forward power the contamination is subtracted.

$$F_{correct} = F_{raw} - C_{for} * R_{correct}$$

The contamination of the forward power is estimated by comparing the forward power in the decay region to the reflected power in that region. The contamination is then subtracted to obtain the corrected forward signal.

3. A complex gain factor relative to the probe and the half-bandwidth of the cavity is estimated by appropriate combinations of the probe, forward power and the time derivative of the probe signal using this equation:

$$Re\left(P * \frac{dP}{dt}\right) = -\omega_{1/2}P * P + \alpha Re(P * F) + \beta(iP * F)$$

The forward power is then scaled by that gain factor:

$$F_{norm} = \left(\frac{\alpha + i\beta}{2\omega_{1/2}}\right)$$

### 3.6.2 RF Based Calibration for R/Q

The voltage induced by a RF generator current or beam current can be described by the equation [11]

$$V_b = \frac{\omega_{1/2}R_L \cdot I}{\omega_{1/2} - j\Delta\omega} \left(1 - e^{-(\omega_{1/2} - j\Delta\omega)t}\right) \quad (3.26)$$

To calibrate  $R/Q$  a short RF pulse is sent into the cavity. This is because for short RF pulses the maximum voltage induced can be approximately written, using equation 3.26, as

$$V_{max} \approx \frac{\omega_{1/2}R_L \cdot I}{\omega_{1/2} - j\Delta\omega} \cdot (\omega_{1/2} - j\Delta\omega)T_B = \omega_{1/2}R_L \cdot IT_B = R_L \cdot I \frac{T_B}{\tau} \quad (3.27)$$

where  $T_B$  is the length of the short RF pulse. Using  $R_L = \frac{1}{2}\left(\frac{R}{Q}\right)Q_L$  and  $\tau = \frac{\omega_0}{2Q_L}$  equation 3.27 becomes

$$V_{max} = \frac{1}{2}\left(\frac{R}{Q}\right)Q_L \cdot I \frac{T_B}{\tau} = \frac{1}{4} \frac{R}{Q} \cdot IT_B\omega_0 \quad (3.28)$$

By sending in short RF pulses with different currents the result can be described by linear regression, i.e. on the form  $y = k \cdot x + m$ .  $k$  is then easily calculated and since  $T_B$  is a known constant,  $R/Q$  can be determined.

If  $R/Q$  is calibrated using a short beam pulse, the induced voltage can be described with equation 3.28 above. As long as  $R/Q$  can be calibrated correctly, the beam induced voltage predicted by the model will more correctly reflect the real value, and hopefully produce a more accurate calibration coefficient. Here  $R/Q$  has to be written as  $R/Q(\beta)$  as it varies for different cavities due to varying beam velocities.

### 3.6.3 Beam Based Calibration for $V_{\text{cav}}$ & Phase

The most common methods of calibrating proton linac phase and amplitude are phase scan methods. Phase scan calibration is done by scanning RF phase and amplitude, measuring beam arrival time at downstream locations, comparing measured phase to model predicted data, and identifying the best-matched data for calibration. Phase scan methods can achieve an accuracy of  $1^\circ$  in phase, and 1 % in amplitude in the low energy part, but struggle to achieve this in the high energy part due to the insensitivity of the high-velocity proton beam to energy gain in the cavity. The alternate way to set phase and amplitude is to use a transient beam loading method, which looks promising to achieve high accuracy as long as high precision measurement can be made.

A general transient beam loading method for phase and amplitude calibration at SNS (a drift beam method) is listed below [14]:

1. Measure accurately beam current and beam pulse shape by BCMs (Beam Current Monitor).
2. Tune the cavity to resonance frequency.
3. Turn off RF. Turn on beam with specified beam current and pulse length.
4. Measure the phase and amplitude of the beam-induced signal.
5. Measure the phase and amplitude of the noise signal before the next beam pulse comes. Subtract noise signal from the beam-induced signal.
6. Repeat the measurement in step (4) for approximately ten beam pulses and average the results.
7. Predict the beam-induced signal in the model by measured beam current and beam pulse shape.
8. Determine the phase offset and amplitude calibration coefficient by comparing measured result with model calculations.
9. Set amplitude and phase.

# Measurements

The measurements were done by applying a RF-signal into a copper cavity and analysing its behaviour. The measurement set up can be seen in figure 4.1. Two different signal generators were used to see if it had any effect on the measurements.

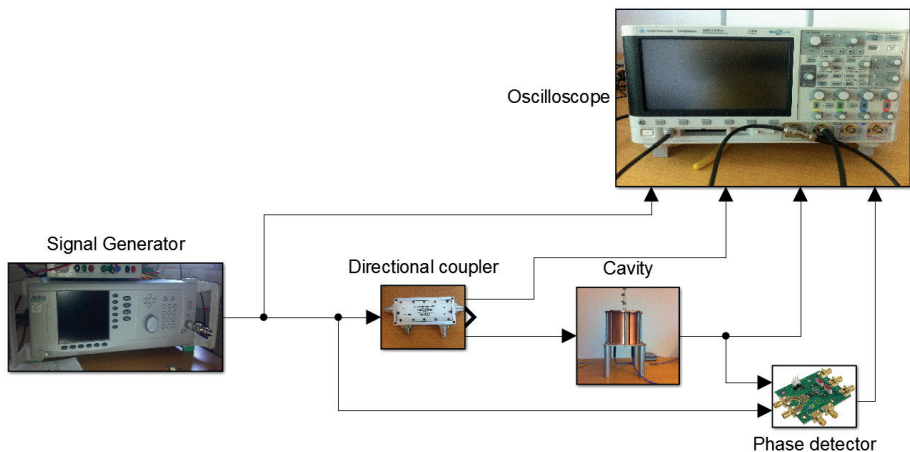


**Figure 4.1:** Measurement setup.

## 4.1 Cavity Response

When the RF-signal pulse is applied to the cavity it takes a while for it to reach the maximum amplitude, as can be seen in figure 4.2. The same happens when the pulse is over, the amplitude decreases and it is during this period that  $Q_L$  can be calculated with equation 3.20.

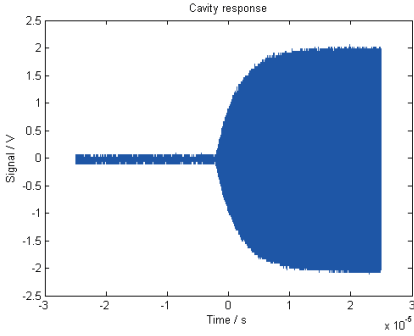


**Figure 4.2:** Cavity response on the rising edge of a pulse.

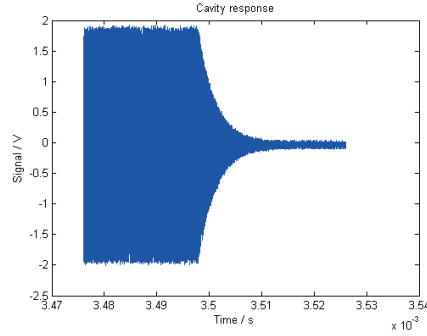


**Figure 4.3:** Cavity response on the falling edge of a pulse.

## 4.2 Detuning Measurement

### 4.2.1 Decay

In order to measure the detuning the phase of the cavity field is needed. The RF/IF Gain and Phase detector AD8302 from Analog Devices is used for the measurements. It compares the phase of two signals and outputs a voltage that corresponds to the difference by using this equation [7]

$$V_{PHS} = V_{\Phi} \cdot (\Phi(V_{INA}) - \Phi(V_{INB})) \Rightarrow V_{PHS} = V_{\Phi} \cdot \Delta\Phi \quad (4.1)$$

where  $V_{INA}$  is the input voltage of one of the input signals,  $V_{INB}$  is the input voltage of the other signal and  $V_{\Phi}$  is the phase slope. To get the phase difference, the phase slope needs to be calculated. This is done by comparing two signals with a known phase difference, then changing one of them and recording the output voltage of the phase detector. The result can be seen in figure 4.4 where two different frequencies, 352.21 MHz and 327.36 MHz, were used. As can be seen the phase slope is different for the two measurements,  $V_{\Phi} = -10.47$  mV/deg for 352.21 MHz and  $V_{\Phi} = -7.23$  mV/deg for 327.36 MHz. This seems to show that the phase slope changes with the frequency. There is a big gap in the measurements for the phase slope in figure 4.4b though, so it is not certain.

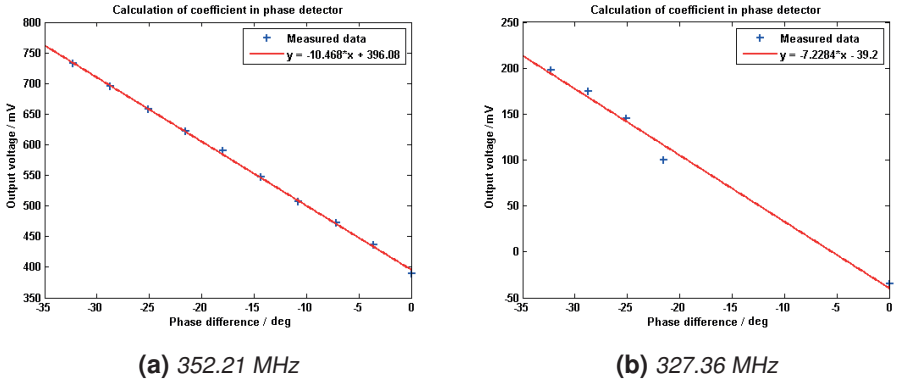


Figure 4.4: Measured voltage for different phase differences at 352.21 MHz and 327.36 MHz.

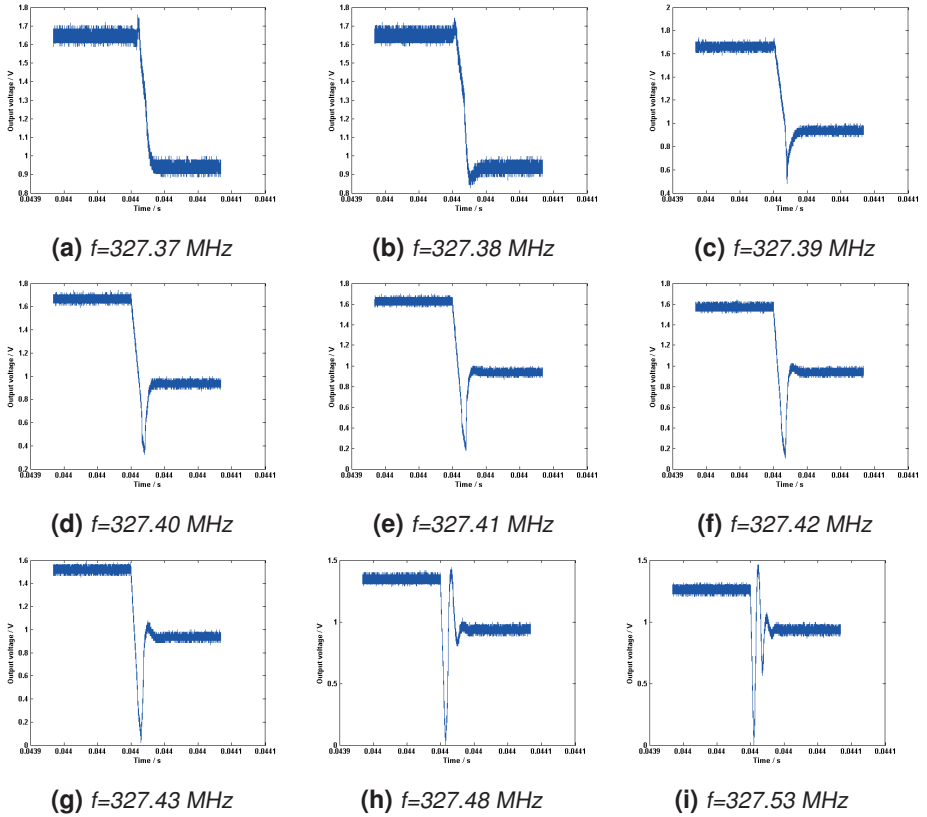


Figure 4.5: The phase of the cavity field at different RF-frequencies.

As described in section 2.4 the detuning after the pulse is calculated using the equation

$$\Delta\omega = \frac{d}{dt}\phi_{cav}$$

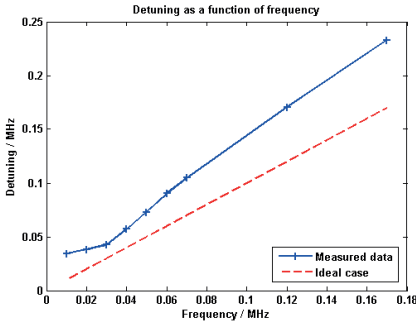
In order to get the detuning from the measured data shown in figure 4.5, where the cavity is tuned to 327.36 MHz, it has to be rewritten, by using equation 4.1, to

$$\Delta\omega = \frac{d}{dt}\Delta\Phi = \frac{dV_{PHS}}{dt} \frac{1}{V_\Phi} \quad (4.2)$$

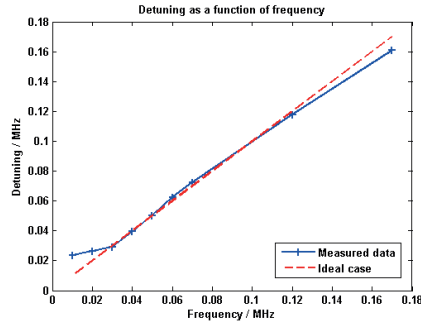
and since  $V_\Phi$  is in mV/deg while  $\Delta\omega$  is in rad/s the result must be multiplied with  $\pi/180$  to convert to the right unit, and the convert it to Hz by dividing with  $\pi$ , which gives the equation

$$\Delta f = \frac{dV_{PHS}}{dt} \frac{1}{V_\Phi} \frac{1}{2 \cdot 180} \quad (4.3)$$

After calculating the slopes for all the frequencies, they were plotted in figure 4.6 using both the phase slopes from before. As can be seen it is almost a linear decrease in detuning which is as it should be. The strange part is that the result is better using the phase slope calculated for 352.21 MHz than using the phase slope calculated for 327.36 MHz, which is the same frequency that the measurements were done at. This can originate from the previously mentioned gap in the measurements using the phase slope of 327.36 MHz.



(a)  $V_\Phi = -7.23$  mV/deg



(b)  $V_\Phi = -10.47$  mV/deg

**Figure 4.6:** How the detuning changes when the frequency is changes.

## 4.3 $Q_L$ Measurement

### 4.3.1 Decay

To calculate the  $Q_L$ -value the decay of the cavity response is used. This is done by taking the logarithm of the decay and using equation 3.20.

The measurements done with the first signal generator can be seen in figure 4.7 and the  $Q_L$  result can be seen in Table 4.1

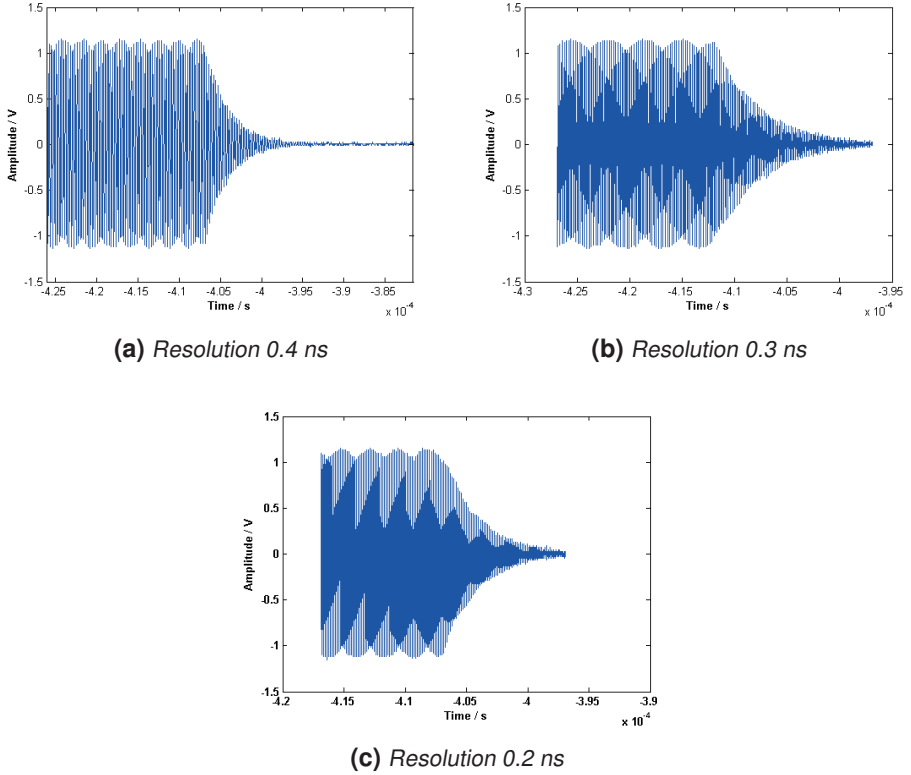


**Figure 4.7:** Decay measurement

**Table 4.1:**  $Q_L$ -values for the different measurements

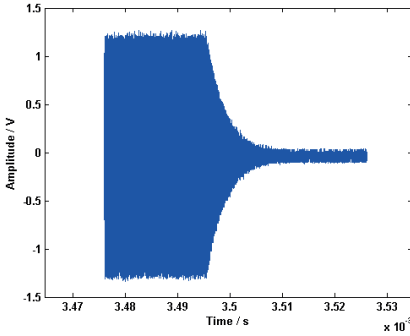
$\tau$	Loaded Q-value, $Q_L$	Resolution (ns)
$2.92 \cdot 10^{-6}$	2946	0.2
$4.32 \cdot 10^{-6}$	4365	0.3
$2.98 \cdot 10^{-6}$	3013	0.4

The purpose of these experiments is to see how  $Q_L$  value measurements are affected by resolution. The resolution here is the interval time between 2 sampling points, which equivalently can be viewed as the reciprocal of sample frequency. Theoretically, SNR will be higher for higher sampling frequencies, as shown in equation 4.4 [15] where  $B$  is the number of bits in the DAC,  $A$  is the amplitude,  $F_{sOS}$  is the oversampling rate and  $F_s$  is the Nyquist sampling rate. But it is also affected by clock jitter, especially in direct sampling for RF frequency. Data shows that  $Q_L$  is indeed affected by the resolution, but there is no relation between the samples. Maybe there is other noise or expected modulations in the experiments. The waveform is studied in a small area, and it is found to be modulated by

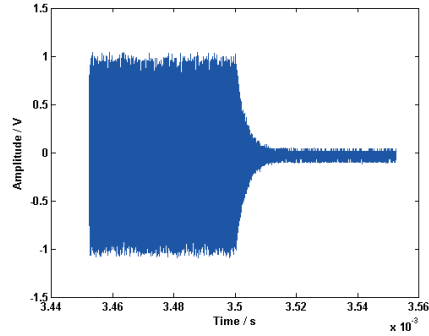


some unknown signal and it may affect the results.

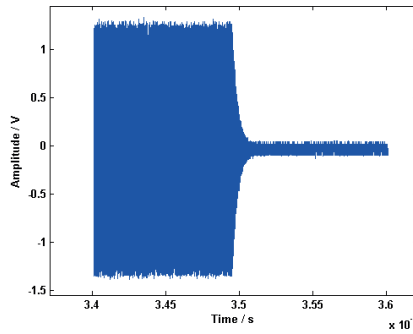
$$SNR = 1.76 + 6.02 \cdot B + 20\log(A) + 10\log(F_{sOS}/F_s) \quad (4.4)$$



(a)  $\tau = 3.57 \cdot 10^{-6}$



(b)  $\tau = 3.86 \cdot 10^{-6}$



(c)  $\tau = 3.64 \cdot 10^{-6}$

**Figure 4.8:** Decay measurement

**Table 4.2:**  $Q_L$ -values for the different measurements

$\tau$	Loaded Q-value, $Q_L$	Resolution (ns)
$3.57 \cdot 10^{-6}$	3676	0.8
$3.86 \cdot 10^{-6}$	3971	1.6
$3.64 \cdot 10^{-6}$	3745	3.2

The measurement done with the second signal generator is shown in figure 4.8 and the  $Q_L$  result can be seen in Table 4.2. In this measurement the signal generator was better. The waveform is much better this time. However, the results is still a bit strange. The middle resolution deviates very much from the other two. Looking at the waveform, the amplitude differs from the other two as well. SNR will also be affected by the amplitude.

Further investigations are made on how  $Q_L$  results are affected by the amplitude. This time the same resolution but different amplitudes are used. The result can be seen in Table 4.3 and 4.4. Since this analysis was not planned from the beginning there is not enough data to draw safe conclusions.

**Table 4.3:**  $Q_L$ -values for the different amplitudes at the first measurement

Amplitude (V)	$Q_L$
1.5	2695
1.2	2770

**Table 4.4:**  $Q_L$ -values for the different amplitudes at the second measurement

Amplitude (V)	$Q_L$
1.8	3512
1.25	3701

The conclusion from the results using different amplitudes is that the  $Q_L$  value should not change much by different amplitude as shown in tables 4.3 and 4.4 above. An interesting result is that the middle resolution deviates much from the other one in both measurements. It may be caused by spikes in the SNR due to some relationship between the sampling frequency and the resonance frequency shown in figure 4.9.

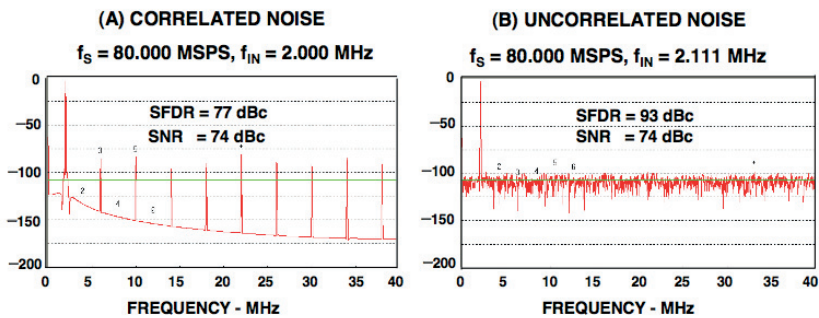


**Figure 4.9:** Effect of ratio of sampling clock to input frequency on quantization noise spectrum for ideal 12-bit ADC [16]

## 4.4 Directivity of Directional Coupler Measurement

Measurements of the directivity are made using a Vector Network Analyzer (VNA). After the initial calibration the directional couplers input port, port one in figure 4.10, is connected to the first port of the VNA and the coupled port, port 2, is connected to the second port in the VNA. The transmitted port was terminated with a  $50 \Omega$  load in order to get no

reflection in the directional coupler.  $S_{12}$  was then measured. Since there is no reflection, the measured value shows the coupling factor. It can be shown using equation 3.8

$$P_{out} = 10^{-C/20} \cdot (P_{for} + 10^{-D/20} \cdot P_{ref}).$$

When  $P_{ref} = 0$  then  $P_{out} = 10^{-C/20} \cdot P_{for}$  which is equivalent to  $P_{out} = P_{for} - C$  in dB and since there is no reflection  $P_{for} = P_{in}$ . This leads to  $P_{out} = P_{in} - C$  in dB.

To get the directivity the first port of the VNA is connected to the transmitted port, port 3, of the directional coupler and the second port of the VNA is connected to the coupled port, port 2. The input port, port 1, is terminated with a  $50 \Omega$  load to remove the reflection in the coupler. Now the input signal will act like the reflected signal and since port 1 is terminated the forward power will be zero. This means that the power measured will be  $P_{out} = 10^{-(C+D)/20} \cdot P_{ref}$  which is equivalent with  $P_{out} = P_{in} - C - D$  in dB. This means that  $D = P_{in} - P_{out} - C$  and since  $P_{in}$  and  $C$  are the same as in the previous measurement, the directivity is calculated as  $D = P_{out,1} - P_{out,2}$ .

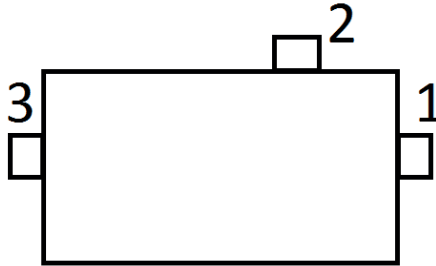


**Figure 4.10:** Sketch of the directional coupler used in the measurements

---

# Conclusion

---

The purpose of this master thesis was to investigate how different factors affect the precision of measurements and if there are any other methods of measuring that gives more accurate values.

There are both advantages and disadvantages with the measurement methods used. The advantage with the method of using the forward and cavity voltage, equation 3.18, is that it is possible to measure the whole detuning curve in one measurement and it is also less sensitive to the directivity than the method of measuring the difference between the forward and cavity voltage. The second measuring method though is less sensitive to a wrong coupling factor value than the voltage method. The method of derivation of the cavity voltage's phase results in the correct detuning in all cases, but only after the pulse, but so does the method of using equation 3.18 with the same result.

The method of using equation 3.18 for measuring the quality factor does work, but not very well. It depends strongly on the directivity and the coupling factor. The old way of calculating it, i.e. using equation 3.20, results within 0.01 % of the input value for both when the directivity is not ideal and when the coupling factor is wrong.

A quite big disadvantage with the method using equation 3.18 for calculating both the detuning and the loaded quality factor is that you have to know one of them to get the other. Since there are other ways to determine the loaded quality factor, which are more easily done and has better accuracy, the method using equation 3.18 is not preferred.

Overall I think that the new way to measure the detuning is better since the coupling factor errors source is a misalignment of the directional coupler and the amplifier and that can more easily be fixed than the directivity of the coupler. To fix the directivity you essentially need to buy a new coupler with better directivity.



---

# References

---

- [1] T. Schilcher, *Vector Sum Control of Pulsed Accelerating Fields in Lorentz Force Detuned Superconducting Cavities*, University of Hamburg, 1998-04-27.
- [2] R. Zeng, *An Introduction to Cavity Control at ESS*, ESS RF Workshop, Uppsala, 2013-12-04
- [3] S. Molloy, R. Zeng, *Some Considerations on Predetuning for Superconducting Cavities*, 2012-03-09.
- [4] <http://www.europeanspallationsource.se/>
- [5] S. Peggs (Ed.), *Technical Design Report*, April, 2013
- [6] K.-J. Kang, Y.-X. Wei, B. Dwersteg, "The Computer Aided Test System for RF Superconducting Cavity High-Q Measurement", in the *Proceedings of the Fifth Workshop on RF Superconductivity*, DESY, Hamburg, Germany, August, 1991
- [7] [http://www.analog.com/static/imported-files/data\\_sheets/AD8302.pdf](http://www.analog.com/static/imported-files/data_sheets/AD8302.pdf)
- [8] S. Michizono, D. Arakawa, S. Fukuda, E. Kako, H. Katagiri, T. Matsumoto, T. Miura, Y. Yano, "Performance of LLRF System at s1-global in KEK" in the *Proceedings of IPAC2011*, p. 451-453, San Sebastian, Spain, September, 2011
- [9] [http://www.markimicrowave.com/Assets/appnotes/directivity\\_and\\_vswr\\_measurements.pdf](http://www.markimicrowave.com/Assets/appnotes/directivity_and_vswr_measurements.pdf)
- [10] R. Zeng, D. McGinnis, S. Molloy, A. J. Johansson, *Control Performance Improvement by Using Feed Forward in LLRF*, 2012-06-04
- [11] R. Zeng, *Power Overhead Reduction for RF Field Control in Beam Commissioning*, 2013-03-14
- [12] A. Brandt, *Development of a Finite State Machine for the Automated Operation of the LLRF Control at FLASH*, University of Hamburg, 2007-05-25
- [13] W. Schappert, Y. Pischalnikov, "Adaptive Compensation Fro Lorentz Force Detuning in Superconducting Cavities", in the *Proceedings of SRF2011*, Chicago, 2011
- [14] H. Padamsee, J. Knobloch, T. Hays, *RF Superconductivity for Accelerators*, John Wiley, New York 1998.
- [15] *A Technical Tutorial on Digital Signal Synthesis*, Analog Devices, 1999

- [16] W. Kester, *Taking the Mystery out of the Infamous Formula, "SNR = 6.02N + 1.76dB," and Why You Should Care*, Analog Devices, 2009
- [17] *TraceWin Manual*, Commissariat à l'Energie Atomique et aux Energies Alternatives (CEA), France.

# Simulink Models

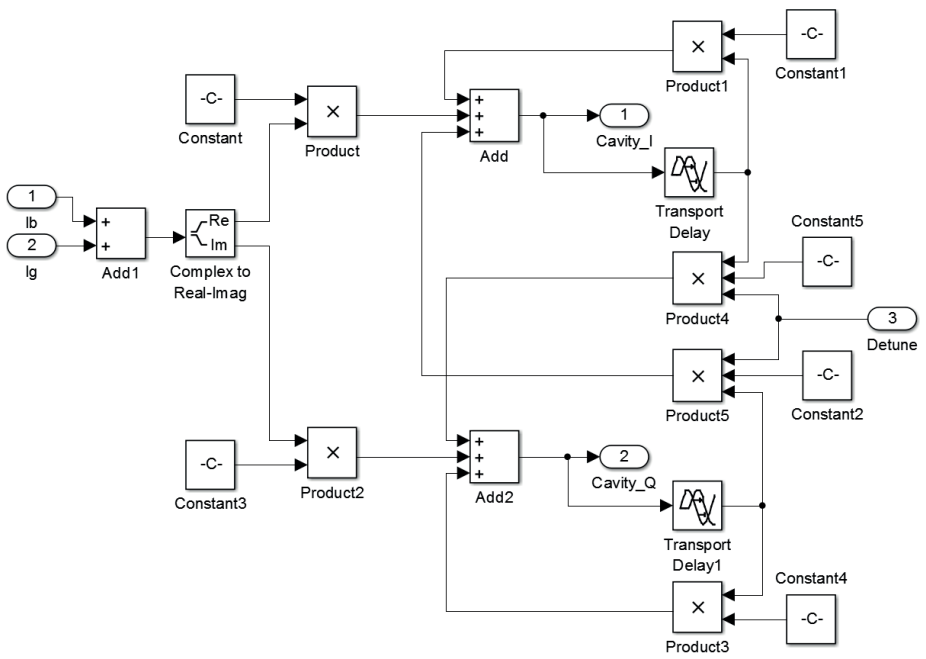


**Figure A.1:** Cavity model in Simulink



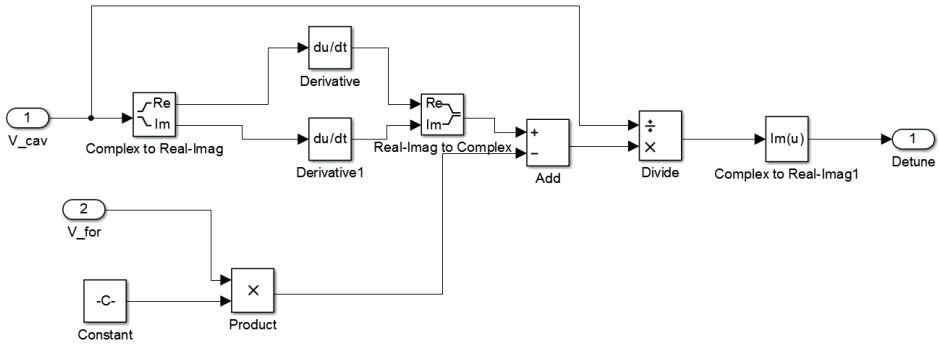


**Figure A.2:** The model of calculating the detuning in Simulink



**LUND**  
UNIVERSITY

Series of Master's theses  
Department of Electrical and Information Technology  
LU/LTH-EIT 2015-425

<http://www.eit.lth.se>